

# UNIVERSITÄTSKLINIKUM HAMBURG-EPPENDORF

Institut für Osteologie und Biomechanik

Prof. Dr. med. Michael Amling

## **Molecular control of bone matrix quality by Wnt1**

### **Dissertation**

zur Erlangung des Grades eines Doktors der Medizin  
an der Medizinischen Fakultät der Universität Hamburg

vorgelegt von

Wenbo Zhao

aus Kunming, Volksrepublik China

Hamburg 2021

**Angenommen von der  
Medizinischen Fakultät der Universität Hamburg am: 13.01.2022**

**Veröffentlicht mit Genehmigung der  
Medizinischen Fakultät der Universität Hamburg.**

**Prüfungsausschuss, der/die Vorsitzende: Prof. Dr. Meliha Karsak**

**Prüfungsausschuss, zweite/r Gutachter/in: Prof. Dr. Thorsten Schinke**

# Contents

<b>1. Introduction .....</b>	<b>1</b>
1.1 The biology of bone .....	1
1.1.1 The development of bone.....	1
1.1.2 Bone anatomy and structures .....	2
1.1.3 Functions of bone.....	2
1.1.4 The composition of bone .....	2
1.1.5 Bone modeling and remodeling.....	4
1.2 WNT-signaling pathway.....	5
1.2.1 Mechanisms of WNT-signaling.....	5
1.2.2 WNT-signaling in bone metabolism.....	6
<b>2. Materials and Methods.....</b>	<b>8</b>
2.1 Materials.....	8
2.1.1 Equipment.....	8
2.1.2 Consumables .....	9
2.1.3 Chemicals .....	10
2.1.4 Special Reagents .....	11
2.1.5 Solutions and buffers .....	11
2.1.6 Commercial Kits .....	11
2.1.7 Genotyping primers.....	11
2.1.8 TaqMan probes .....	12
2.1.9 Primary and secondary antibodies for Western-Blotting .....	12
2.1.10 Software .....	13
2.2 Methods.....	13
2.2.1 Animals .....	13
2.2.2 Genotyping.....	14
2.2.3 Mouse skeleton preparation .....	16
2.2.4 Micro-computed tomography (micro-CT/ $\mu$ CT).....	16
2.2.5 Histology and histologic staining .....	17
2.2.6 Structural histomorphometry analysis .....	17
2.2.7 Cell culture .....	17
2.2.8 Isolation of bone marrow-derived osteoblasts .....	18
2.2.9 Isolation of calvarial osteoblasts.....	19
2.2.10 reWnt1/Sfrp1 and reSfrp1 stimulation .....	19
2.2.11 Transfection .....	20
2.2.12 Expression analysis.....	20
2.2.13 Mineralization analysis .....	21
2.2.14 Protein extraction from bones of mice .....	22
2.2.15 Western-Blotting and Ponceau S staining.....	23

<b>3. Results</b> .....	<b>25</b>
3.1 <i>Wnt1</i> has a strong osteoanabolic impact independent of <i>Fzd9</i> in mice .....	25
3.2 Bone marrow-derived osteoblasts react to reWnt1/Sfrp1 stimulation via canonical Wnt-signaling in the absence of <i>Fzd9</i> .....	27
3.3 reWnt1/Sfrp1 stimulation induced the canonical Wnt-signaling pathway in ST2 cells .....	28
3.4 reWnt1/Sfrp1 significantly induced osteogenic differentiation of ST2 cells .....	29
3.5 <i>Omd</i> and <i>Postn</i> were not consistently induced in long bone and calvaria of <i>Wnt1</i> -transgenic mice .....	30
3.6 A pathogenic <i>Wnt1</i> mutation (G177C) impairs the impact of <i>Wnt1 in vitro</i> .....	32
3.7 Stimulation of calvarial or bone marrow-derived osteoblasts with reWnt1/Sfrp1 did not increase <i>Postn/Omd</i> expression or osteogenesis.....	33
3.8 The differential responses of ST2 and MC3T3 cells towards reWnt1/Sfrp1 stimulation may be related to differential expression of putative Wnt1 receptors .....	38
<b>4. Discussion</b> .....	<b>40</b>
<b>5. Summary</b> .....	<b>45</b>
<b>6. Zusammenfassung</b> .....	<b>46</b>
<b>7. Abbreviations</b> .....	<b>47</b>
<b>8. References</b> .....	<b>49</b>
<b>9. Acknowledgements</b> .....	<b>55</b>
<b>10. Publications</b> .....	<b>56</b>
<b>11. Lebenslauf</b> .....	<b>57</b>
<b>12. Eidesstattliche Versicherung</b> .....	<b>58</b>

# 1. Introduction

Bone is a highly specialized tissue of the vertebrate animal body, which consists of inorganic components as well as numerous proteins and bone cells. Some bones offer protection to the organs, such as skull and ribs.<sup>1</sup> Together with cartilage, ligaments and muscles, bones constitute the musculoskeletal system, providing the basis of support and movement to the human body.<sup>1,2</sup> The skeleton develops during embryogenesis and undergoes modeling process. Another process, bone remodeling, consisting of bone formation by osteoblasts and bone resorption by osteoclasts, occurs throughout the human life, contributing to the maintenance of skeletal integrity.<sup>3</sup> Skeletal development and bone remodeling are highly complex processes involving countless factors and biological activities of other systems. Alterations of one or several of the associated factors can result in skeletal diseases or even affect other systems. Examples for such disorders are osteoporosis, osteoporosis-pseudoglioma syndrome (OPPG) and sclerosteosis.<sup>3-6</sup> WNT-signaling, a crucial and complex pathway in numerous biological processes, plays important roles in skeletal development and bone metabolism.<sup>7</sup> Disturbance of WNT-signaling causes various skeletal diseases such as early-onset osteoporosis (EOOP) and osteogenesis imperfecta (OI).<sup>8</sup> While tragic for the affected patients, these diseases provide a rare opportunity to investigate the mechanisms of WNT-signaling in different contexts and find new potential medications for WNT-signaling associated diseases as well as other, more common skeletal disorders such as osteoporosis.

## 1.1 The biology of bone

### 1.1.1 The development of bone

The development of the skeleton begins at the embryonic stage, in which the initial skeletogenesis occurs with the migration of mesenchymal cells derived from different types of embryonic lineages to the sites of future bones.<sup>9</sup> There are two ways to form the bones: intramembranous ossification and endochondral ossification. Intramembranous ossification occurs with the differentiation of mesenchymal stem cells into osteoblasts to directly form bones during the formation of flat bones and part of the clavicle.<sup>1</sup> Endochondral ossification takes place in the cartilage models formed by chondrocytes which are derived from mesenchymal stem cells, predominantly contributing to the formation of long bones.<sup>9,10</sup> During endochondral ossification, the cartilage is gradually replaced by mineralized bone. In the center of the cartilage anlage, the proliferating chondrocytes shift into a non-proliferative hypertrophic state, followed by the invasion of blood vessels, osteoprogenitors, and osteoclasts.<sup>9</sup> Perichondrial cells adjacent to hypertrophic chondrocytes become osteoblasts and form the bone collar, which will form the cortical bone afterwards.<sup>11</sup> The hypertrophic cartilage is then resorbed and the primary ossification center is formed,<sup>1,9</sup> while the proliferative chondrocytes continue proliferating, thus lengthening the bone.<sup>11</sup> As the ossification progresses, the primary ossification center expands, in which the medullary cavity forms subsequently.<sup>9</sup> The secondary ossification center forms in one or both ends of growing bones, followed by the formation of the epiphyseal growth plate, which is

crucial for bone elongation.<sup>1</sup> The growth plate becomes thinner with age and is eventually replaced by bone after puberty.<sup>9</sup>

### **1.1.2 Bone anatomy and structures**

Bones can be classified into four categories according to their shapes: long bones, short bones, flat bones and irregular bones.<sup>2</sup> Long bones, such as femur and tibia, are comprised of diaphysis, metaphysis below the growth plate, and epiphyses above the growth plate.<sup>2</sup> The diaphysis is a hollow shaft composed of mostly dense cortical bone, whereas the metaphysis and epiphyses are composed of trabecular bone and a surrounding thinner shell of cortical bone.<sup>2,10</sup> In contrast, flat bones, including skull, scapula, or ribs, primarily consist of the outer cortical shell with some trabecular structures inside.<sup>10</sup> The structure of short bones and irregular bones is partially similar to flat bones. Overall, 80% of the human skeleton is comprised of cortical bone and 20% of trabecular bone by weight. However, different bones contain different ratios of trabecular and cortical bone.<sup>2</sup>

Histologically, there are two types of bones: woven bone and lamellar bone. Woven bone mainly exists in the embryonic skeleton and is eventually replaced by lamellar bone in the adult skeleton with different structures in trabecular or cortical bone.<sup>10</sup> Collagen fibrils are highly organized and packed in lamellar patterns in trabecular and cortical bones, making the bones strong, and forming the basic structural units of trabecular and cortical bone, which are known as packets and osteons respectively.<sup>2,10</sup>

### **1.1.3 Functions of bone**

It is commonly known that the basic functions of bone include motion of the body, support and protection of soft tissues and organs, storage of calcium and phosphate, maintenance of mineral homeostasis and acid-base balance, as well as harboring the bone marrow.<sup>2,12</sup> Moreover, it has been demonstrated that bone also has endocrine functions.<sup>13</sup> For instance, osteocytes are able to produce fibroblast growth factor 23 (FGF23), thus regulating phosphate and vitamin D metabolism.<sup>14,15</sup> Osteocalcin produced by osteoblasts plays a role in the regulation of glucose, energy metabolism, and testosterone.<sup>16-18</sup> Of note, previous studies demonstrated that the skeletal and immune system interact with each other, although the detailed mechanisms remain unclear.<sup>19</sup> It is highly possible that future interactions between the skeleton and other systems will be identified in the future.

### **1.1.4 The composition of bone**

Bone consists of bone cells and bone matrix. Bone cells make up approximately 10% of the total bone volume, while bone matrix makes up the residual 90%.<sup>10</sup>

Bone cells include osteoblasts, bone lining cells and osteocytes which are derived from mesenchymal stem cells, and osteoclasts which originate from hematopoietic stem

cells.<sup>1</sup>

Osteoblasts, which make up 4 to 6 percent of total bone cells, are responsible for the formation of bone matrix. They display a cuboidal morphology and are distributed in groups along the bone surfaces.<sup>12</sup> Osteoblasts possess abundant rough endoplasmic reticulum and a prominent Golgi apparatus, which enables them to synthesize large amounts of proteins efficiently.<sup>1,12</sup> With the expression of the most crucial transcription factors such as Runx2 and Osterix, the progenitors from mesenchymal stem cells differentiate to preosteoblasts,<sup>1</sup> which show an increased activity of alkaline phosphatase (ALP) that is necessary for the mineralization of bone matrix.<sup>12</sup> After the maturation of osteoblasts, they begin to secrete type-I collagen and bone matrix proteins such as osteocalcin (OCN), bone sialoprotein (BSP) and osteopontin.<sup>12,20</sup> Next, this organic bone matrix termed osteoid is mineralized by the integration of hydroxyapatite crystals, completing the bone formation.<sup>12,21</sup> Subsequently, the matured osteoblasts will be embedded into the newly formed bone matrix and differentiate into osteocytes, or remain on the bone surface as bone lining cells, or undergo apoptosis.<sup>22</sup>

Bone lining cells are derived from osteoblasts, which are flattened and distribute on endocortical and trabecular bone surfaces.<sup>1,12</sup> In contrast to osteoblasts, bone lining cells have much less cytoplasmic organelles and synthetic activity.<sup>1,12</sup> Moreover, neither bone resorption nor bone formation occurs on the surfaces beneath these cells.<sup>12</sup> Cytoplasmic processes which extend to canaliculi are observed on some of these cells,<sup>1,12</sup> possibly communicating with osteocytes in the bone matrix.<sup>1</sup> Bone lining cells are also found to be linked with each other and adjacent osteoblasts.<sup>2,12</sup> Bone lining cells are thought to be quiescent osteoblasts, nevertheless, they are still capable to be activated into osteoblasts.<sup>23</sup> Furthermore, It was demonstrated that they are able to produce OPG and RANKL, two key regulators of osteoclastogenesis.<sup>1,23</sup> During bone remodeling cycles, these cells are important components of the basic multicellular units.<sup>12</sup>

Osteocytes are the most abundant cells in bone, comprising 90 to 95 percent of all the bone cells.<sup>20</sup> Osteocytes are derived from osteoblasts. At the end of active bone formation, some osteoblasts differentiate to osteocytes that are located within the bone matrix in voids termed lacunae.<sup>12</sup> Osteocytes are completely embedded in bone matrix. As they were difficult to isolate in early studies, they were considered as quiescent cells.<sup>12,20</sup> In fact, osteocytes form a massive network in the bone matrix via their processes and play an essential role in signaling and regulation of other bone cells.<sup>1</sup> During the differentiation from osteoblasts to osteocytes, the cytoplasmic processes gradually emerge and eventually spread through the canaliculi, thus forming the osteocyte lacunocanicular system. The total cell surface of the osteocyte network is estimated to be 400-fold larger than that of the Haversian and Volkmann system, and 100-fold larger than that of trabecular bone surface.<sup>12,20,24</sup> Through the extensive connection in the skeleton, osteocytes act as mechanosensors, detecting mechanical loads and strains on bones, which enables the skeleton to adapt to the mechanical pressures.<sup>1,12,20</sup> Furthermore, osteocytes were found to be the main source of RANKL

to induce osteoclastogenesis.<sup>25</sup>

Osteoclasts are large and multinucleated cells that facilitate the resorption of bone matrix and are located in Howship lacunae also known as resorption lacunae.<sup>10</sup> Osteoclasts are derived from the hematopoietic stem cell lineage and are under the control of several key factors. Macrophage colony-stimulating factor (M-CSF), which is secreted by osteoprogenitor mesenchymal cells and osteoblasts among other cells, stimulates the proliferation of osteoclast precursors when binding to its receptor.<sup>12,26</sup> RANKL, mostly expressed by osteoblasts and osteocytes, promotes osteoclastogenesis when binding to its receptor RANK in osteoclast precursors.<sup>1,12</sup> On the other hand, osteoprotegerin (OPG), which is produced by osteoblasts, stromal cells, and gingival and periodontal fibroblasts, acts as a decoy receptor of RANKL, preventing the RANKL/RANK interaction, thus suppressing osteoclastogenesis.<sup>1,12,27</sup> The clear zone and the ruffled border are the most characteristic morphological features of matured osteoclasts. They delineate the area where the resorption lacunae are formed.<sup>1,12,28</sup> In the ruffled border, proton pumps such as vacuolar proton ATPase (V-ATPase) and chloride channels facilitate the acidification of the resorption lacunae, causing the dissolution of the calcium phosphate crystals of the bone matrix. Together with proteases such as cathepsin K and matrix metalloproteinase-9 (MMP-9) that digest the organic components of the bone matrix, bone resorption occurs.<sup>1,12,29</sup>

Apart from all the bone cells, bone matrix comprises up to 90% of the bone tissue volume.<sup>10</sup> Bone matrix consists of inorganic and organic components, as well as a small amount of lipids and water.<sup>2,12</sup> Collagenous proteins make up approximately 90% of the organic matrix, which contains predominantly type-I collagen. Non-collagenous proteins include osteocalcin (OCN), osteopontin, bone sialoprotein (BSP), osteonectin, bone morphogenetic proteins (BMPs).<sup>12</sup> Phosphate and calcium ions are the main components of the inorganic matrix, which form the hydroxyapatite crystals and subsequently deposit into the scaffold made up of collagens and non-collagenous proteins.<sup>30</sup> Furthermore, bicarbonate, sodium, potassium, citrate, magnesium, carbonate, fluoride, zinc, barium, and strontium are also important trace elements found in the inorganic matrix.<sup>12,31</sup>

### **1.1.5 Bone modeling and remodeling**

Bone modeling and remodeling are both crucial processes in the skeleton, which determine the bone structures and components.<sup>1</sup> Bone modeling occurs from the beginning of skeletal development until approximately the age of 20 years, during which bone formation and bone resorption take place independent of each other, mainly contributing to the longitudinal growth of the skeleton and changes in bone morphology.<sup>1,2</sup> In contrast, in bone remodeling, bone formation and bone resorption are coupled tightly. Bone remodeling takes place in bone sites that require to be remodeled, which entails removal of old bone packets and the subsequent synthesis of new bone, thus continuously refreshing the skeleton throughout life.<sup>1,2,12</sup>

The initial phase of the remodeling cycle is the recruitment of hematopoietic stem cells to the specific remodeling sites, which is regulated by osteoclastogenic factors such as RANKL and M-CSF.<sup>25,32</sup> Bone lining cells that cover the surfaces of bones are lifted, followed by the fusion of multiple mononuclear cells to form multinucleated preosteoclasts, which consequently differentiate to matured osteoclasts.<sup>2</sup> Bone remodeling occurs at sites of temporary structures termed basic multicellular units (BMUs), which consist of a group of osteoclasts to form the cutting cone followed by a group of osteoblasts to form the closing cone.<sup>1,12</sup> The bone resorption process takes approximately 3 weeks in adult human bones, whereas the bone formation lasts 3 to 6 months.<sup>1,2</sup>

Bone remodeling replaces 5 to 10 percent of the skeleton per year in adult humans, with a cortical turnover rate of 2 to 3 percent per year. This process continuously replaces old bone with fresh bone and repairs the microdamage, thus maintaining the mechanical strength of the skeleton.<sup>2,30</sup>

## 1.2 WNT-signaling pathway

### 1.2.1 Mechanisms of WNT-signaling

A mutation in the gene *Wingless* was found to cause the loss of wings in *Drosophila melanogaster* in 1976.<sup>33</sup> In 1982, it was demonstrated that mouse mammalian tumor virus is able to insert a DNA copy of its RNA genome at a specific site of the genome of mammary cells, which results in breast cancer in mice.<sup>34</sup> The putative proto-oncogene was named *Int1*. However, in 1987 the *Drosophila* homologue of *Int1* was proved to be identical to *Wingless*.<sup>35</sup> With this recognition, a new nomenclature was initiated and the Wnt family was established, which is a group of secreted glycoproteins.<sup>36</sup>

After the establishment of the Wnt family proteins, the mechanism of the signaling pathway involving WNTs as ligands was widely investigated. So far, three patterns of WNT-signaling were established: the canonical WNT-signaling pathway, as well as noncanonical pathways including the WNT-planar cell polarity (WNT-PCP) pathway, and the WNT-calcium (WNT-Ca<sup>2+</sup>) pathway.<sup>37</sup>

The Canonical WNT-signaling pathway is most thoroughly established. The signaling pattern is relatively clear, which is based on the complex of a WNT ligand, a transmembrane co-receptor from the low density lipoprotein receptor-related protein (LRP) family and a main receptor from the frizzled (FZD) family, with  $\beta$ -catenin as the intracellular signal. However, different LRPs (LRP4/5/6), 19 identified WNTs and 10 FZDs make the actual signaling pathway highly complex.<sup>38</sup> In the absence of WNT ligands, intracellular  $\beta$ -catenin is continuously targeted by the multiprotein destruction complex, which consists of axin, glycogen synthase kinase 3 (GSK3), adenomatous polyposis coli (APC) and casein kinase 1 (CK1), thus causing the phosphorylation of  $\beta$ -catenin. This leads to the polyubiquitination of  $\beta$ -catenin by E3 ubiquitin ligase and subsequent degradation by proteasome.<sup>37</sup> With a low level of intracellular  $\beta$ -catenin, T

cell factor/lymphoid enhancer factor (TCF/LEF) transcription factors are suppressed by Groucho in the nucleus so that WNT-signaling is not induced.<sup>38</sup> When a canonical WNT ligand binds LRP5/6 and a FZD receptor, Dishevelled (DSH) will be recruited to FZD, which results in the binding of Axin to the LRP5/6 tail.<sup>7,37</sup> This recruits GSK3 and Frequently Rearranged in Advanced T-Cell Lymphoma 1 (FRAT1), thus inhibiting the multiprotein destruction complex and abolishing the phosphorylation of  $\beta$ -catenin. This in turn prevents  $\beta$ -catenin from proteosomal degradation.<sup>38</sup> Following the accumulation in cytoplasm,  $\beta$ -catenin translocates into the nucleus, where it interacts with the TCF/LEF transcription factors and causes them to separate from the repressor Groucho.<sup>37,39</sup> Eventually, WNT-signaling downstream target genes such as *AXIN2* and *APCDD1* are transcribed.<sup>7</sup>

Noncanonical WNT-signaling also involves the binding of WNT ligands to FZD receptors. However, the intracellular signal is transduced in a different way independent of  $\beta$ -catenin.<sup>38,40</sup> The planar cell polarity pathway (WNT-PCP pathway) regulates different kinds of cellular behaviours including planar cell polarity, cell movement during gastrulation and neural crest cell migration.<sup>38,40</sup> In the WNT-PCP pathway, WNT ligands bind to FZD as well as receptor tyrosine kinase-like orphan receptor 2 (ROR2) or receptor-like tyrosine kinase (RYK) transmembrane co-receptors, which recruits DSH to FZD, followed by the association with dishevelled-associated activator of morphogenesis 1 (DAAM1).<sup>37</sup> The formation of this complex activates the small G-protein RHO, followed by activation of RHO-associated kinase (ROCK), which plays an important role in regulating the cytoskeleton.<sup>38</sup> Alternatively, DSH associates with another small G-protein RAC, activating c-Jun N-terminal kinases (JNK), thus interacting with JNK pathway.<sup>41</sup> Another noncanonical WNT-signaling pathway is termed WNT-calcium pathway (WNT/ $\text{Ca}^{2+}$  pathway), in which the binding of WNT ligands to FZD recruits DSH, subsequently activating the heterotrimeric G-proteins and leading to the activation of phospholipase C (PLC). Then the formation of inositol triphosphate (IP3) and diacylglycerol (DAG) occurs. IP3 leads to the release of  $\text{Ca}^{2+}$  into the cytoplasm by binding to its receptor on the endoplasmic reticulum. The increased cytoplasmic  $\text{Ca}^{2+}$  concentration activates calcium/calmodulin-dependent kinase II (CamKII) that in turn facilitates cellular activities such as cell adhesion and migration by the subsequent activation of Nuclear factor of activated T-cells (NFAT).<sup>38,40</sup> On the other hand, DAG activates protein kinase C (PKC) and mitogen-activated protein kinases (MAPKs), which then regulate numerous other cellular activities such as modulation of the canonical WNT-signaling pathway.<sup>38,42</sup>

### **1.2.2 WNT-signaling in bone metabolism**

WNT-signaling participates in lots of biological activities, including the determination of cell fate and proliferation in embryonic development and tissue homeostasis. The dysregulation of WNT-signaling has been found to be associated with numerous types of cancers in humans.<sup>7</sup> Furthermore, WNT-signaling also plays essential roles in bone metabolism.<sup>37,38</sup>

First of all, both canonical and non-canonical WNT-signaling are very important for skeletal development.<sup>37</sup> Compound mutations in both *Lrp5* and *Lrp6* were proven to cause limb defects in mice.<sup>43</sup> Mutations in *LRP4* were reported to result in syndactyly in humans,<sup>44</sup> while homozygous *Lrp4*-deficient mice were found to display fully penetrant polysyndactyly in fore and hind limbs.<sup>45</sup> *Wnt5a* and its co-receptor *Ror2* were demonstrated to be crucial for skeletal development, whereas the disruption of these can cause Brachydactyly type B (BDB1) and Robinow syndrome (RRS).<sup>46</sup>

WNT-signaling influences activities of all bone cells during bone metabolism. For instance, WNT-signaling directly supports osteoblastic lineage commitment by repressing mesenchymal stem cell commitment to chondrogenic and adipogenic lineages.<sup>47-49</sup> The activation of non-canonical Wnt-signaling by *Wnt5a* promotes osteoclastogenesis.<sup>50</sup> The common WNT antagonists *SOST* and *DKK1*, which are primarily produced by osteocytes, bind to *LRP5/6* to repress WNT-signaling in osteoblasts and reduce bone formation.<sup>37</sup> Moreover, in the late stage of bone resorption during bone remodeling, osteoclasts may recruit osteoprogenitors to the remodeling site and then promote osteoblast differentiation and osteogenesis through the crosstalk between BMP and Wnt-signaling.<sup>51</sup>

When observed from a macroscopic view, some of the 19 known WNT ligands of mammals significantly affect bone mass. *Wnt10b* was revealed to induce osteoblast differentiation and to inhibit adipogenesis through canonical Wnt-signaling.<sup>52,53</sup> *Wnt16* deficiency in mice results in thinner and more porous cortical bone as well as increased fracture risk while interestingly trabecular bone remains unaffected. On the other hand, osteoblast-specific overexpression of human *WNT16* in mice lead to higher bone mass in both trabecular and cortical bone compartments.<sup>54,55</sup> Moreover, the previous study of our group showed that the osteoblast-specific *Wnt1* overexpression induced a significant and rapid increase of bone mass in mice.<sup>56</sup>

Disruptions of WNT-signaling can cause various diseases of skeleton, such as OPPG, sclerosteosis and Van Buchem disease (VBD).<sup>39,57</sup> Similarly, WNT1 mutations in humans result in a series of skeletal diseases.<sup>8,58,59</sup> Since the mechanism of WNT1 in bone metabolism remains unclear, the main goal of this study is to investigate how exactly WNT1 affects skeletal integrity.

## 2. Materials and Methods

### 2.1 Materials

#### 2.1.1 Equipment

Equipment	Model/Version	Manufacture
Analytical balance	CPA224S	Sartorius AG, Göttingen, DE
Analytical balance	TE2101	Sartorius AG, Göttingen, DE
Camera	EOS 200D	Canon Inc., Tokyo, JP
Camera lens	50mm 1:2.8 Macro	Sigma Corp., Kawasaki, JP
Cell culture incubator	BBD 6220	Heraeus GmbH, Hanau, DE
Centrifuge	GS-6	Beckman Coulter Inc., Brea, US
Centrifuge	5415D	Eppendorf AG, Hamburg, DE
Centrifuge	5430R	Eppendorf AG, Hamburg, DE
Centrifuge	5425	Eppendorf AG, Hamburg, DE
Class II biological safety cabinet	MSC-Advantage™	Thermo Fisher Scientific Inc., Waltham, US
Cold light platform	LP5000K	Hama GmbH & Co. KG, Monheim, DE
Electrophoresis cell	Sub-Cell GT	Bio-Rad Laboratories, Inc., Hercules, US
Incubation bath	1012	GFL Gesellschaft für Labortechnik GmbH, Burgwedel, DE
Incubator shaker	Innova 4000	New Brunswick Scientific Co., Inc., Edison Township, US
Magnetic Stirrer	RCT Basic	IKA GmbH & Co. KG, Staufen im Breisgau, DE
MicroCT scanner	µCT 40	Scanco Medical AG, Brüttisellen, CH
Microplate reader	VersaMax™	Molecular Devices, San Jose, US
Microprocessor controlled power supply	200/2.0	Bio-Rad Laboratories, Inc., Hercules, US
Microscope	Axioskop	Carl Zeiss AG, Oberkochen, DE
Microscope	IX50	Olympus Corp., Tokyo, JP
Molecular Imager ChemiDoc™ XRS System	170-8070	Bio-Rad Laboratories, Inc., Hercules, US
PCR cycler	Msastercycler® pro S	Eppendorf AG, Hamburg, DE
Precision balance	440-33	Kern & Sohn GmbH, Balingen, DE
Scanner	G4050	HP Inc., Palo Alto, US

<b>Equipment</b>	<b>Model/Version</b>	<b>Manufacture</b>
Shaker	Duomax 1030	Heidolph Instruments GmbH & Co. KG, Schwabach, DE
Spectrophotometer	ND1000	PEQLAB Biotechnologie GmbH, Erlangen, DE
StepOnePlus Real-Time PCR System	StepOnePlus	Applied Biosystems Inc., Waltham, US
Thermomixer	Thermomixer comfort	Eppendorf AG, Hamburg, DE
Tube roller	RS-TR05	Phoenix Instrument GmbH, Garbsen, DE
Vilber E-box Imaging system	VX2	Vilber, Marne-la-Vallée, FR
Western-Blotting system	Mini Gel Tank system	Thermo Fisher Scientific Inc., Waltham, US
Western-Blotting system	Mini Bolt Module	Thermo Fisher Scientific Inc., Waltham, US
X-ray cabinet	621/96	Faxitron, Tucson, US
X-ray film processor	1170-1-0000	PROTEC GmbH & Co. KG, Oberstenfeld, DE

## 2.1.2 Consumables

<b>Consumables</b>	<b>Manufacture</b>
100 Sterican® needles	B. Braun Melsungen AG, Melsungen, DE
1.5 ml SafeSeal micro tube	Sarstedt AG & Co. KG, Nürmbrecht, DE
12-well cell culture plate	Greiner Bio-One GmbH, Kremsmünster, AT
2.0 ml SafeSeal micro tube	Sarstedt AG & Co. KG, Nürmbrecht, DE
Biosphere® Filter Tips 0.1-10 µl	Sarstedt AG & Co. KG, Nürmbrecht, DE
Biosphere® Filter Tips 100-1000 µl	Sarstedt AG & Co. KG, Nürmbrecht, DE
Biosphere® Filter Tips 2-100 µl	Sarstedt AG & Co. KG, Nürmbrecht, DE
Cell culture flask, 250 ml, 75 cm <sup>2</sup>	Greiner Bio-One GmbH, Kremsmünster, AT
Injekt®-F	B. Braun Melsungen AG, Melsungen, DE
MicroAmp™ Fast Optical 96-Well Reaction Plate	Thermo Fisher Scientific Inc., Waltham, US
Microtiter plate	Sarstedt AG & Co. KG, Nürmbrecht, DE
Nitrocellulose transfer membrane 0.45µm pore size	Schleicher & Schuell Inc., Keene, US
PCR SingleCap 8-pack SoftStrips 0.2 ml	Biozym Scientific GmbH, Hessisch Oldendorf, DE
PCR SoftStrips 12, 0.2 ml	Biozym Scientific GmbH, Hessisch Oldendorf, DE
Pierce™ Protein Concentrators 10K MWCO	Thermo Fisher Scientific Inc., Waltham, US
Quality Pipette Tips 0.1-10 µl	Sarstedt AG & Co. KG, Nürmbrecht, DE

<b>Consumables</b>	<b>Manufacture</b>
Quality Pipette Tips 100-1000 µl	Sarstedt AG & Co. KG, Nürmbrecht, DE
Quality Pipette Tips 2-200 µl	Sarstedt AG & Co. KG, Nürmbrecht, DE
Sarstedt® cells craper	Sarstedt AG & Co. KG, Nürmbrecht, DE
Serological pipette 10 ml	Sarstedt AG & Co. KG, Nürmbrecht, DE
Serological pipette 25 ml	Sarstedt AG & Co. KG, Nürmbrecht, DE
Serological pipette 5 ml	Sarstedt AG & Co. KG, Nürmbrecht, DE
Slide-A-Lyzer™ G2 Dialysis Cassette	Thermo Fisher Scientific Inc., Waltham, US

### 2.1.3 Chemicals

<b>Chemical name</b>	<b>Abbreviation</b>	<b>Molecular formula</b>	<b>Manufacture</b>
Acetic Acid		CH <sub>3</sub> COOH	Carl Roth GmbH & Co. KG, Karlsruhe, DE
Alizarin Red S		C <sub>14</sub> H <sub>7</sub> NaO <sub>7</sub> S	Sigma-Aldrich Corp., St. Louis, US
Ammonium hydroxide		NH <sub>4</sub> OH	Sigma-Aldrich Corp., St. Louis, US
Diethyl pyrocarbonate	DEPC	C <sub>6</sub> H <sub>10</sub> O <sub>5</sub>	Sigma-Aldrich Corp., St. Louis, US
Dimethyl sulfoxide	DMSO	(CH <sub>3</sub> ) <sub>2</sub> SO	Carl Roth GmbH & Co. KG, Karlsruhe, DE
Ethylenediaminetetra acetic acid	EDTA	C <sub>10</sub> H <sub>16</sub> N <sub>2</sub> O <sub>8</sub>	Sigma-Aldrich Corp., St. Louis, US
Ethanol	EtOH	C <sub>2</sub> H <sub>6</sub> O	Merck KGaA, Darmstadt, DE
Ethidium bromide	EtBr	C <sub>21</sub> H <sub>20</sub> BrN <sub>3</sub>	Sigma-Aldrich Corp., St. Louis, US
Guanidine·HCl		CH <sub>5</sub> N <sub>3</sub> ·HCl	SERVA Electrophoresis GmbH, Heidelberg, DE
L-Ascorbic acid	ASC	C <sub>6</sub> H <sub>8</sub> O <sub>6</sub>	Sigma-Aldrich Corp., St. Louis, US
Methanol	MeOH	CH <sub>3</sub> OH	Carl Roth GmbH & Co. KG, Karlsruhe, DE
Tris(hydroxymethyl)aminomethane	Tris	(HOCH <sub>2</sub> ) <sub>3</sub> CN 2	Carl Roth GmbH & Co. KG, Karlsruhe, DE
Tween 20		C <sub>58</sub> H <sub>114</sub> O <sub>26</sub>	Carl Roth GmbH & Co. KG, Karlsruhe, DE
β-glycerophosphate	β-Gly	C <sub>3</sub> H <sub>9</sub> O <sub>6</sub> P	Sigma-Aldrich Corp., St. Louis, US
β-mercaptoethanol	βME	HOCH <sub>2</sub> CH <sub>2</sub> SH	Sigma-Aldrich Corp., St. Louis, US

## 2.1.4 Special Reagents

Reagents	Manufacture
Bovine Albumin standard	Thermo Fisher Scientific Inc., Waltham, US
cOmplete™ Protease Inhibitor Cocktail	Roche AG, Basel, CH
G418-BC	Biochrom GmbH, Berlin, DE
reWnt1/Sfrp1 (9765-WN)	R&D Systems, Minneapolis, US
reSfrp1 (9019-SF)	R&D Systems, Minneapolis, US

## 2.1.5 Solutions and buffers

Name	Composition
TAE buffer (50×)	2M Tris-Base 1M acetic acid 100mM EDTA ad H <sub>2</sub> O pH=8.5 (adjust with HCl if necessary)
Extraction buffer (For bone protein extraction)	4M Guanidine 0.5 M EDTA 50 mM Tris 1× protease inhibitor cocktail pH=7.4 (adjust with HCl if necessary)

## 2.1.6 Commercial Kits

Kit name	Manufacture
Phire Animal Tissue Direct PCR Kit	Thermo Fisher Scientific Inc., Waltham
Lipofectamine LTX & PLUS Reagent Kit	Invitrogen Corp., Waltham, US
Macherey-Nagel NucleoSpin RNA/Protein Kit	Macherey-Nagel, GmbH & Co. KG, Düren, DE
peqGOLD TriFast Kit	PEQLAB Biotechnologies GmbH, Erlangen, DE
Verso cDNA Synthesis Kit	Thermo Fisher Scientific Inc., Waltham, US
GeneChip™ WT PLUS Reagent Kit	Thermo Fisher Scientific Inc., Waltham, US

## 2.1.7 Genotyping primers

Primer	Sequence
Wnt1-Luc	For (5' CGC CAA AAA CAT AAA GAA AGG C 3') Rev (5' TGT CCC TAT CGA AGG ACT CTG G 3')
ColtTA	For (5' CTC TGC ACC TTG GTG ATC 3') Rev (5' GCT GCT TAA TGA GGT CGG 3')

Primer	Sequence
Fzd9 WT	For v2 (5' CTT CCT CTG CTC GCT CTA CG 3') Rev v2 (5' GTG CAG CCT GTG TTT TCC AG 3')
Fzd9 KO	For (5' ATA GCC TGA AGA ACG AGA TCA 3') Rev v2 (5' CCC CCT GTG TCT CAC TTG TC 3')

### 2.1.8 TaqMan probes

Gene	Catalog number
<i>Gapdh</i>	4352661
<i>Axin2</i>	Mm00443610_m1
<i>Apcdd1</i>	Mm01257559_m1
<i>Omd</i>	Mm00449589_m1
<i>Postn</i>	Mm00450111_m1
<i>Tnfsf11</i>	Mm00441908_m1
<i>Tnfrsf11b</i>	Mm00435454_m1
<i>Wnt1</i>	Mm01300555_g1
<i>Alpl</i>	Mm00475834_m1
<i>Bglap</i>	Mm03413826_mH
<i>Ibsp</i>	Mm00492555_m1
<i>Runx2</i>	Mm00501580_m1
<i>Sp7</i>	Mm00504574_m1
<i>Col1a1</i>	Mm00801666_g1
<i>Lrp4</i>	Mm00554326_m1
<i>Lrp5</i>	Mm01227476_m1
<i>Lrp6</i>	Mm00999795_m1
<i>Fzd1</i>	Mm00445405_s1
<i>Fzd2</i>	Mm02524776_s1
<i>Fzd3</i>	Mm00445423_m1
<i>Fzd4</i>	Mm00433382_m1
<i>Fzd5</i>	Mm00445623_s1
<i>Fzd6</i>	Mm00433387_m1
<i>Fzd7</i>	Mm00433409_s1
<i>Fzd8</i>	Mm01234717_s1
<i>Fzd9</i>	Mm01206511_s1
<i>Fzd10</i>	Mm00558396_s1

### 2.1.9 Primary and secondary antibodies for Western-Blotting

Antibody	Source	Dilution	Manufacture	Product number
Omd	Goat	1:2000	R&D Systems, Minneapolis, US	AF3308

Antibody	Source	Dilution	Manufacture	Product number
Col1a1	Rabbit	1:1000	Kerafast Inc., Boston, US	ENH018-FP
Rabbit Anti-Goat Immunoglobulins/HRP	Rabbit	1:1000	Dako GmbH, Hovedstaden, DK	P0449
Goat Anti-Rabbit Immunoglobulins/HRP	Goat	1:2000	Dako GmbH, Hovedstaden, DK	P0448

## 2.1.10 Software

Software	Version	Manufacture
Microsoft Office 2010	16.0	Microsoft Corp., Redmond, US
EndNote	X7	Thomson ResearchSoft, Stanford, US
GraphPad Prism	8.0.1	GraphPad Software Inc. San Diego, US
StepOne™ Software	2.3	Applied Biosystems Inc., Waltham, US
Bioquant Osteo	7.00.10	BIOQUANT Image Analysis Corp., Nashville, US
MicroCT Analysis Software	4.05	Scanco Medical AG, Brüttisellen, CH
Quantity One Software	4.6.9	Bio-Rad Laboratories, Inc., Hercules, US
Image Studio Lite	5.2	LI-COR Biosciences, Lincoln, US

## 2.2 Methods

### 2.2.1 Animals

*Col1a1<sup>tTA</sup>/pTet<sup>Wnt1</sup>/Fzd9<sup>+/+</sup>* and *Col1a1<sup>tTA</sup>/pTet<sup>Wnt1</sup>/Fzd9<sup>-/-</sup>* mice (STOCK-Tg(tetO-*Wnt1*, -luc)TWNTLach-Tg(Col1a1-tTa)139Niss-*Fzd9*<sup>tm1Uta/Uke</sup>) were used for analysis. *Col1a1<sup>tTA</sup>/pTet<sup>Wnt1</sup>/Fzd9<sup>-/-</sup>* mice were generated by crossing the mice which possess an osteoblast-specific inducible transgenic *Wnt1* gene with *Fzd9*-deficient mice. Both mouse colonies were described in details in the previous studies.<sup>56,60</sup>

The mice were housed in a pathogen-free environment with a 12-hour light/dark cycle, 45% to 65% relative humidity and temperature in the range of 20 °C to 24 °C in open or individually ventilated cages with proper nesting materials. The mice had *ad libitum* access to tap water and standard rodent chow (1328P, Altromin Spezialfutter GmbH & Co. KG, Lage, DE). The mice were always kept under the diet that contained doxycycline (ssniff-Spezialdiäten GmbH, Soest, DE) unless being specifically ordered. The removal of doxycycline from the diet lasted for 7 days in *Col1a1<sup>tTA</sup>/pTet<sup>Wnt1</sup>/Fzd9<sup>+/+</sup>* and *Col1a1<sup>tTA</sup>/pTet<sup>Wnt1</sup>/Fzd9<sup>-/-</sup>* groups. An additional group of *Col1a1<sup>tTA</sup>/pTet<sup>Wnt1</sup>/Fzd9<sup>+/+</sup>* mice was always kept under the diet with doxycycline as control.

## 2.2.2 Genotyping

The genotypes of mice were identified by polymerase chain reaction (PCR) and agarose gel electrophoresis. Tail biopsies were obtained from newborn mice. DNA was extracted using the Phire Animal Tissue Direct PCR Kit (Thermo Fisher Scientific Inc., Waltham, US; 20µl Dilution Buffer and 0.5µl DNA Release Additive for each sample) at room temperature for 5 min followed by the incubation of 2 min at 98°C.

The sequences of the primers are listed in the section “Genotyping primers” above. The PCR protocols and thermocycler settings used for genotyping are listed in Table 1 to Table 4.

After completing the PCR, samples were loaded on a 1% agarose gel in Tris-acetate-EDTA buffer (TAE buffer) with Ethidium bromide (EtBr, 10mg/ml, use 5µl/100ml gel, Sigma-Aldrich Corp., St. Louis, US), and underwent electrophoresis at the voltage of 120V for 25 minutes. A DNA ladder (GeneRuler 1 kb Plus DNA Ladder, Thermo Fisher Scientific Inc., Waltham, US) was used for identifying the sizes of the PCR products. The gels were visualized with ultraviolet light by using the Vilber E-box Imaging system (Vilber, Marne-la-Vallée, FR).

**Table 1. PCR protocols for genotyping**

<b>Wnt1 Tg</b>			
Component	Volume (µl)	PCR Program	
H <sub>2</sub> O	12.5	Initialization	94°C 4 min
10× Dream Taq Green Buffer	2.5	Denaturation	94°C 30 sec
DMSO	0.25	Annealing	52°C 40 sec
dNTPs (10mM)	0.5	Elongation	72°C 1 min
Primer1 (Wnt1-Luc For, 2 pMol/µl)	4	Last Elongation	72°C 10 min
Primer2 (Wnt1-Luc Rev, 2 pMol/µl)	4	Store	4°C
Dream Taq DNA Polymerase	0.25	Target band: 500bp	
DNA	1 (≈50ng)		
Total	25		

**Table 2. PCR protocols for genotyping**

<b>ColtTA</b>			
Component	Volume (μl)	PCR Program	
H <sub>2</sub> O	12.5	Initialization	94°C 5 min
10×Dream Taq Green Buffer	2.5	Denaturation	94°C 30 sec
DMSO	0.25	Annealing	60°C 30 sec
dNTPs (10mM)	0.5	Elongation	72°C 30 sec
Primer1 (Col-tTA For, 2 pMol/μl)	4	Last Elongation	72°C 7 min
Primer2 (Col-tTA Rev, 2 pMol/μl)	4	Store	4°C
Dream Taq DNA Polymerase	0.25	Target band: 550bp	
DNA	1 (≈50ng)		
Total	25		

**Table 3. PCR protocols for genotyping**

<b>Fzd9 WT</b>			
Component	Volume (μl)	PCR Program	
H <sub>2</sub> O	8.2	Initialization	94°C 4 min
10×Dream Taq Green Buffer	2	Denaturation	94°C 40 sec
DMSO	2	Annealing	58°C 40 sec
dNTPs (10mM)	0.5	Elongation	72°C 1 min
Primer1 (Fzd9 WT For v2, 2 pMol/μl)	3	Last Elongation	72°C 10 min
Primer2 (Fzd9 WT Rev v2, 2 pMol/μl)	3	Store	4°C
Dream Taq DNA Polymerase	0.3	Target band: 600bp	
DNA	1 (≈50ng)		
Total	20		

**Table 4. PCR protocols for genotyping**

<b>Fzd9 KO</b>			
Component	Volume (μl)	PCR Program	
H <sub>2</sub> O	8.2	Initialization	94°C 4 min
10×Dream Taq Green Buffer	2	Denaturation	94°C 40 sec
DMSO	2	Annealing	58°C 40 sec
dNTPs (10mM)	0.5	Elongation	72°C 1 min
Primer1 (Fzd9 KO For, 2 pMol/μl)	3	Last Elongation	72°C 10 min
Primer2 (Fzd9 KO Rev v2, 2 pMol/μl)	3	Store	4°C
Dream Taq DNA Polymerase	0.3	Target band: 250bp	
DNA	1 (≈50ng)		
Total	20		

### 2.2.3 Mouse skeleton preparation

The mice were sacrificed for analysis at the age of 6 weeks, before which doxycycline had been removed from the diet for 7 days or maintained in the diet until sacrifice as indicated. Mice were euthanized with 100% CO<sub>2</sub> after anesthesia with a mixture of 20% O<sub>2</sub> and 80% CO<sub>2</sub>. Blood samples were obtained through heart-puncture by using a syringe and serum was collected after 6 min of centrifugation at 3,300 rcf. The skin and organs in thoracic and abdominal cavities were removed without damaging the skeleton of the mice. Mice were fully stretched and fixed on a cork-board, and then fixed by submersion in 3.7% PBS-buffered formaldehyde for 48 hours. After fixation, the mice were transferred into 80% ethanol for temporary storage. Contact radiographs were prepared using an X-ray cabinet (35kV, 2s, Faxitron, Tucson, US) and X-ray films (AGFA Corp., Mortsel, NL) that were developed using an automated X-ray processor (PROTEC GmbH & Co. KG, Oberstenfeld, DE). The tibiae and femora of the right side and the lumbar spines (L1 to L4) of the mice were isolated without damaging the structure. All bones were stored in 80% ethanol until further analysis.

### 2.2.4 Micro-computed tomography (micro-CT/μCT)

The right femora of mice were analyzed by micro-CT after fixation. The femora were fixed into a sample holder and the micro-CT scan was conducted with a voxel resolution of 10μm by using the μCT 40 system (Scanco Medical AG, Brüttisellen, CH)

according to the manufacturer's guidelines. Trabecular bone was analyzed in a volume within 500 $\mu$ m to 2500 $\mu$ m proximal of the distal growth plate. Cortical bone was analyzed in a volume within 1000 $\mu$ m in the middle of the diaphysis using the Scanco  $\mu$ CT evaluation software suite. Parameters obtained included trabecular bone volume (BV/TV, bone volume/tissue volume), trabecular Tissue mineral density (Tb. TMD), cortical thickness (Ct. Th) and cortical porosity (Ct. Por). 3D models were generated by the same analysis system.

### **2.2.5 Histology and histologic staining**

The fixed right tibiae and lumbar spines (L1 to L4) of mice were dehydrated by ascending ethanol concentrations. Afterwards the bones were embedded in methyl methacrylate. Sectioning and staining were performed routinely by the histology lab of the Department of Osteology and Biomechanics (IOBM, UKE). Sections of 4 $\mu$ m thickness were cut in the sagittal (tibia) or coronal (spine) plane and stained by von Kossa/van Gieson staining.

### **2.2.6 Structural histomorphometry analysis**

Sections of tibiae and lumbar spines after von Kossa/van Gieson staining were used for structural histomorphometry analysis with Bioquant Osteo (BIOQUANT Image Analysis Corp., Nashville, US). Images of sections were taken by microscope (Carl Zeiss AG, Oberkochen, DE) with a magnification of 1.25 $\times$  and a resolution of 3900 $\times$ 3090. Lumbar vertebrae L3 and L4 were selected for analysis, in which the trabecular bone within vertebral bodies was quantified with a threshold of 110 in the red channel. The mean value of the parameters of vertebrae L3 and L4 was recorded, including trabecular bone volume (BV/TV, bone volume/tissue volume), trabecular number (Tb. N), trabecular thickness (Tb. Th) and trabecular separation (Tb. Sp). The trabecular bone distal of the proximal growth plate of tibiae was quantified with the same threshold, of which the length along the axis of tibia was approximately equal to the length of the proximal growth plate.

### **2.2.7 Cell culture**

The ST2 cell line (obtained from Leibniz Institute DSMZ, Braunschweig, DE), the MC3T3 cell line (ATCC, Manassas, US), bone marrow-derived osteoblasts and calvarial osteoblasts were utilized for *in vitro* analysis.

The ST2 cell line displays mesenchymal characteristics and is derived from the bone marrow of mice. ST2 cells can be induced to differentiate into osteoblasts in response to ascorbic acid and  $\beta$ -glycerophosphate (both from Sigma-Aldrich Corp., St. Louis, US). In this study, the ST2 cell line was used for reWnt1/Sfrp1 or reSfrp1 stimulation, transfection, gene expression analysis and receptor expression analysis.

The MC3T3 cell line is an osteoblastic cell line derived from mouse calvaria, which is

capable to differentiate into mineralizing osteoblasts. The MC3T3 cell line was utilized for reWnt1/Sfrp1 or reSfrp1 stimulation and receptor expression analysis in this study.

Bone marrow-derived osteoblasts were isolated from wildtype and *Fzd9*<sup>-/-</sup> mice and were used for gene expression analysis and reWnt1/Sfrp1 and reSfrp1 stimulation.

Calvarial osteoblasts were isolated from wildtype new born mice and were utilized for reWnt1/Sfrp1 and reSfrp1 stimulation.

MC3T3 cells were cultured in Minimum Essential Medium Eagle (Alpha modification, Sigma-Aldrich Corp., St. Louis, US). Minimum Essential Medium Eagle (Alpha modification, powder, Sigma-Aldrich Corp., St. Louis, US) was reconstituted and used for the ST2 cell line, bone marrow-derived osteoblasts and calvarial osteoblasts. The medium was supplemented with 10% fetal calf serum (FCS, Lonza Group, Basel, CH) and 1% antibiotics (Penicillin/Streptomycin, 10,000 U/ml, Thermo Fisher Scientific Inc., Waltham, US). All cells were maintained at 37°C in an atmosphere with 5% CO<sub>2</sub> and a relative humidity of 95%. The medium was changed on every Monday, Wednesday and Friday. Osteogenic differentiation was induced and maintained by adding 50µg/ml ascorbic acid and 10mM β-glycerophosphate (Sigma-Aldrich Corp., St. Louis, US) to the medium. Trypsin/EDTA (0.25%, Thermo Fisher Scientific Inc., Waltham, US) was used to detach the cells during passages. All the cells were passaged when they reach a confluence of 90% to 100%.

### **2.2.8 Isolation of bone marrow-derived osteoblasts**

Bone marrow-derived osteoblasts were isolated from wildtype and *Fzd9*<sup>-/-</sup> mice at the age of 6 weeks. Mice were sacrificed by the same method as indicated above. Femora, tibiae and hip bones were obtained and temporarily stored on ice. All the bones were transferred into the clean bench and a PCR tube with a small hole in the bottom was fixed into an Eppendorf tube beforehand for the centrifugation to remove the bone marrow. The femora were cut proximal to the distal growth plate while the tibiae were cut through the distal joint of tibia and fibula. The hip bones were cut above the acetabulum to the side of ischium and pubis. All the bones were loaded into the PCR tubes with the open side downwards. Bone marrow was removed by a transient centrifugation at 6,000 rcf for 12 s and then gathered and diluted with 500µl warm αMEM +/+ (supplemented with 10% fetal calf serum (FCS) and 1% antibiotics (Penicillin/Streptomycin)) medium (Sigma-Aldrich Corp., St. Louis, US) per tube. The solution was filtered through a filter (70µm, Greiner Bio-One GmbH, Kremsmünster, AT) and the filter was washed by extra 2ml of αMEM +/+ medium. Cell counting was performed with a cell counting chamber (LO - Laboroptik Ltd., Lancing, GB) according to the manufacturer's guidelines. Cells were diluted according to the cell counting result and then loaded into 12-well cell culture plates (Greiner Bio-One GmbH, Kremsmünster, AT) with a concentration of 5 million cells/ml. The medium was changed for the first time 2 days after plating the cells.

## 2.2.9 Isolation of calvarial osteoblasts

Calvarial osteoblasts were isolated from newborn mice at the age of 3 to 5 days. After sacrifice by decapitation, the calvaria were prepared in a clean bench followed by careful removal of soft tissues. The calvaria were temporarily stored in sterile PBS. Digestion buffer was prepared and warmed up to 37°C before use, which consisted of 1mg/ml collagenase (Sigma-Aldrich Corp., St. Louis, US), 2mg/ml dispase (Dispase® II, Roche AG, Basel, CH) and  $\alpha$ MEM -/- (without supplement of serum or antibiotics) medium (30ml, enough for 5 mice, Sigma-Aldrich Corp., St. Louis, US). Before the incubation, the digestion buffer was filtered through a filter (0.2 $\mu$ m, Th. Geyer GmbH & Co. KG, Renningen, DE) in the clean bench. The calvaria were incubated in 10 to 12ml digestion buffer (enough for 5 mice) at 37°C for 12 min with simultaneous shaking at 200 rpm. After completing the initial digestion, the digestion buffer was removed and replaced by fresh digestion buffer, followed by a further digestion at 37°C for 50 min with simultaneous shaking at 200 rpm. After the second digestion, the solution was filtered in the bench through a filter (70 $\mu$ m, Greiner Bio-One GmbH, Kremsmünster, AT) and the filter was flushed with extra 2ml of  $\alpha$ MEM +/+ medium. The filtered solution was centrifuged at 400 rcf for 6 min followed by removal of the liquid without touching the cell layer. The cells were resuspended with fresh, prewarmed  $\alpha$ MEM +/+ medium and cell counting was performed as indicated above. Cells were plated in 12-well cell culture plates (Greiner Bio-One GmbH, Kremsmünster, AT) with a concentration of 50,000 cells/ml.

## 2.2.10 reWnt1/Sfrp1 and reSfrp1 stimulation

reWnt1/Sfrp1 (Recombinant Mouse Wnt-1/sFRP-1 Complex, 9765-WN, R&D Systems, Minneapolis, US) and reSfrp1 (Recombinant Mouse sFRP-1, 9019-SF, R&D Systems, Minneapolis, US) were utilized for the stimulation experiments. Both reagents were reconstituted to a concentration of 100 $\mu$ g/ml with sterile PBS. ST2 cells were loaded into 12-well cell culture plates (Greiner Bio-One GmbH, Kremsmünster, AT) with a concentration of 100,000 cells/ml, while the concentration was 50,000 cells/ml for MC3T3 cells and calvarial osteoblasts, and 5 million cells/ml for bone marrow-derived osteoblasts. For the short-term stimulation, after the cells reached 80% confluence, they were serum starved with  $\alpha$ MEM -/- medium for 16 h. Then the cells were treated for 6 h with fresh  $\alpha$ MEM -/- medium which contained PBS (final concentration=1 $\mu$ l/ml) or reWnt1/Sfrp1 (final concentration=100ng/ml) or reSfrp1 (final concentration=50ng/ml). For the long-term stimulation, 50  $\mu$ g/ml ascorbic acid and 10 mM  $\beta$ -glycerophosphate (both from Sigma-Aldrich Corp., St. Louis, US) were added into the  $\alpha$ MEM +/+ medium to induce and maintain osteogenic differentiation, during which PBS (final concentration=1 $\mu$ l/ml) or reWnt1/Sfrp1 (final concentration=100ng/ml) or reSfrp1 (final concentration=50ng/ml) were added to treat the cells. During the long-term stimulation process, medium was changed on every Monday, Wednesday and Friday.

## 2.2.11 Transfection

ST2 cells were used for transient and stable transfection utilizing the Lipofectamine LTX & PLUS Reagent Kit (Invitrogen Corp., Waltham, US) according to manufacture guidelines. ST2 cells were loaded into 12-well cell culture plate (Greiner Bio-One GmbH, Kremsmünster, AT) with a concentration of 100,000 cells/ml. The transfection was performed one day after plating the cells. Optimized volumes of the reagents are listed in Table 5. For transient transfection, the medium was removed one day after the transfection. The cells were washed by 1ml/well PBS once and then underwent osteogenic differentiation for 5 days, followed by RNA isolation and expression analysis by qRT-PCR. For stable transfection, after removal of medium and washing with PBS, G418-BC (Biochrom GmbH, Berlin, DE) was added into the medium with a concentration of 300U/ml for selection for 5 days, during which the medium with G418-BC was changed every two days. After selection, the cells were detached and re-plated, followed by a recovery period for the cells until they reached 80% confluence. Subsequently, osteogenic differentiation was started and maintained for 15 days as indicated above, after which Alizarin red staining and corresponding mineralization quantification were performed as indicated in the section “Mineralization analysis” below.

**Table 5. Optimized volumes of reagents for transfection**

Transfection reagent for each well		
<b>Reagent A</b>	$\alpha$ MEM -/-	50 $\mu$ l
	LTX	2 $\mu$ l
<b>Reagent B</b>	$\alpha$ MEM -/-	50 $\mu$ l
	DNA Plasmid	1 $\mu$ g
	PLUS Reagent	1 $\mu$ l

## 2.2.12 Expression analysis

RNA was isolated from cultured cells by using the Macherey-Nagel NucleoSpin RNA/Protein Kit (Macherey-Nagel, GmbH & Co. KG, Düren, DE) according to the manufacturer guidelines. For the isolation of RNA from bones, long bones (femora and tibiae) and calvaria of mice were prepared. Long bones were separated from mice and the muscles and other soft tissues were removed. Calvaria were prepared with careful removal of the soft tissues. The bone samples were grinded to a fine powder in liquid nitrogen. Then the peqGOLD TriFast Kit (PEQLAB Biotechnologies GmbH, Erlangen, DE) was used for RNA isolation according to the manufacturer guidelines. The purity and concentration of the RNA samples was measured utilizing the spectrophotometer (ND-1000, PEQLAB Biotechnologie GmbH, Erlangen, DE) according to the instructions. The Verso cDNA Synthesis Kit (Thermo Fisher Scientific Inc., Waltham, US) was utilized to synthesize cDNA according to manufacture instructions. The reaction protocol is listed in Table 6. For qRT-PCR, the TaqMan system (Applied

Biosystems Inc., Waltham, US) and StepOnePlus Real-Time PCR System (Applied Biosystems Inc., Waltham, US) were used for reaction mixture and PCR reaction respectively. The components of TaqMan system are listed in Table 7. The information of TaqMan probes is listed in the section “TaqMan probes” above. The PCR reaction was performed for 40 cycles. Afterwards, the  $\Delta\Delta CT$  method was used for analysis. Whole transcriptome analysis was performed by using the Clariom D, mouse system (Thermo Fisher Scientific Inc., Waltham, US) according to the manufacturer’s GeneChip™ WT PLUS Reagent Kit user guide. The signals were analyzed with the Transcriptome Analysis Console (TAC) software (Thermo Fisher Scientific Inc., Waltham, US) according to the manufacture’s user guide.

**Table 6. Protocol for cDNA synthesis**

Components	Volume (µl) 1×
5× cDNA Synthesis Buffer	2
dNTP Mix (5 mM)	1
Anchored Oligo dT (500 ng/µL)	0.5
Verso Enzyme Mix	0.5
RT Enhancer	0.5
H <sub>2</sub> O	1.5*
RNA	4*
<b>Total</b>	10
42°C 30min → 95°C 2min → Dilute with H <sub>2</sub> O according to cDNA concentration (2 to 4 times)	
* Adjust according to RNA concentration. Maximum RNA amount is 500ng.	

**Table 7. Reaction components for qRT-PCR**

Components	Volume (µl) 1×
TaqMan™ Gene Expression Master Mix	10
TaqMan™ Primer	1
cDNA	2*
H <sub>2</sub> O	7*
<b>Total</b>	20
* Adjust according to RNA and cDNA concentration. Common amount of cDNA is 20ng.	

### 2.2.13 Mineralization analysis

Alizarin red staining and corresponding quantification were used for mineralization analysis. For Alizarin red staining, all the medium was removed from cells. For 12-well plate, all the wells were washed with 1ml/well of PBS. Then cells were fixed with 1ml/well of cold 90% ethanol for 15 min. Afterwards, ethanol was removed and all the wells were washed twice with 1ml/well of water. Cells were stained with 1ml/well of the

staining solution (40mM Alizarin red S in H<sub>2</sub>O, pH=4.1~4.2) for 10 min. After staining, all the solution was removed and all the wells were washed with 1ml/well of water for 3 to 5 times based on the intensity of the staining. Before taking pictures, all the liquid was removed. If necessary, the stained plate would be stored with 1ml/well of PBS at 4°C. For the quantification, after removal of the liquid, all the wells were incubated in 800µl/well of 10% acetic acid in H<sub>2</sub>O for 30 min at room temperature. Cell layers were lifted with scrapers and transferred with the liquid into new Eppendorf tubes, followed by incubation at 85°C for 10 min. Afterwards the samples were centrifuged for 10 min at 21,000 rcf. Then 400µl liquid from the top of the centrifuged samples was transferred to new Eppendorf tubes with 150µl of 10% ammonium hydroxide inside. If the mixed solution is deep red with flaky color particles inside, more acetic acid would be added until the solution turned yellow. The same amount of acetic acid was required to be added into all the samples that were to be compared. Subsequently, 150µl mixed liquid was transferred to a microtiter plate (Sarstedt AG & Co. KG, Nürmbrecht, DE) for the absorption reading at 405nm using a Microtiter plate reader (Molecular Devices, San Jose, US). Equivalent volumes of 10% acetic acid in H<sub>2</sub>O and 10% ammonium hydroxide were used as blank control.

#### **2.2.14 Protein extraction from bones of mice**

Femora and tibiae were prepared after the mice were sacrificed. A PCR tube with a small hole in the bottom was fixed into an Eppendorf tube in the clean bench in advance. All the bones were transferred into the clean bench. Epiphyses were cut off and flushed with PBS twice to remove the bone marrow and were kept as trabecular samples. The diaphyses were loaded into the PCR tubes and centrifuged as indicated above to remove the bone marrow and were kept as cortical samples. All the prepared bones were temporarily stored in liquid nitrogen. The bones were carefully grinded to a fine powder in liquid nitrogen and then mixed sufficiently with the extraction buffer (2ml per sample, consisting of 4M Guanidine, 0.5 M EDTA, 50 mM Tris/HCl, pH 7.4 + 1× protease inhibitor cocktail) by using a disperser (Ultra-Turrax<sup>®</sup> T25, IKA GmbH & Co. KG, Staufen im Breisgau, DE). The mixture was incubated at 4°C for 96h with simultaneous shaking, followed by a centrifugation at 1,000 rcf for 20 min at 4°C. The supernatant was collected as the initial extraction while the residues were further incubated with fresh extraction buffer in the same conditions as above for 48h. The samples were centrifuged at 15,000 rcf for 20 min at 4°C and the supernatant was collected and mixed with the initial extraction. The Pierce<sup>™</sup> Protein Concentrators (10K MWCO, Thermo Fisher Scientific Inc., Waltham, US) were used for concentrating the samples to a volume of approximately 1.5ml. Afterwards, the extraction was dialyzed against water using the Slide-A-Lyzer<sup>™</sup> G2 Dialysis Cassette (2K MWCO, Thermo Fisher Scientific Inc., Waltham, US) according to the manufacturer guidelines. The dialyzed samples were concentrated again by using the concentrators. The final volume was approximately 500µl.

The concentration of the samples was measured by Bradford protein assay. The Bovine Albumin standard (BSA, 2mg/ml, Thermo Fisher Scientific Inc., Waltham, US)

was diluted 1:10 with water to reach a concentration of 0.2mg/ml. The dilution protocol for the solution for standard curve is listed in Table 8. Then 200µl Protein Assay Dye Reagent Concentrate (Bio-Rad Laboratories, Inc., Hercules, US) was added into each solution followed by short vortexing. For all the samples, 790µl water and 200µl Protein Assay Dye Reagent Concentrate were mixed with 10µl protein sample followed by transient vortex. Subsequently, 100µl mixed liquid was transferred to a microtiter plate (Sarstedt AG & Co. KG, Nürmbrecht, DE) for the absorption reading at 595nm utilizing a microtiter reader (Molecular Devices, San Jose, US). The actual concentration of the protein samples was calculated according to the standard curve and the volume of samples used for the mixture.

**Table 8. Dilution protocol for the standard BSA solutions**

<b>BSA (µg)</b>	<b>Diluted BSA standard (0.2mg/ml) (µl)</b>	<b>H<sub>2</sub>O (µl)</b>
<b>0</b>	0	800
<b>5</b>	25	775
<b>10</b>	50	750
<b>15</b>	75	725
<b>20</b>	100	700

### 2.2.15 Western-Blotting and Ponceau S staining

Western-Blotting was performed by using the Bolt™ 12% Bis-Tris, 1.0 mm×10 well gel and the matched reagents (Invitrogen Corp., Waltham, US) for preparing samples. The amount of protein for each well was 20µg. The Bolt™ MES SDS Running Buffer (Life Technologies, Carlsbad, US) and Mini Gel Tank system (Thermo Fisher Scientific Inc., Waltham, US) were used for electrophoresis according to the manufacture guideline. The Mini Bolt Module, Mini Gel Tank system (Thermo Fisher Scientific Inc., Waltham, US) and Bolt™ Transfer Buffer (Life Technologies, Carlsbad, US) were used for protein transfer. Nitrocellulose transfer membrane (0.45µm pore size, Schleicher & Schuell Inc., Keene, US) was used during protein transfer. Specifically, the electrophoresis lasted for 30min at 180V, while the protein transfer lasted for 60min at 10V. Transfer buffer was always supplemented with 10% methanol. Nitrocellulose transfer membrane was always soaked into transfer buffer for 5min before use. After protein transfer, the membrane was washed with TBST for 5min for 3 times. The membrane was stained with Ponceau S solution for 10min with gentle shaking, followed by washing with TBST for 5min for 2 to 3 times until the bands were clear. After taking pictures, the membrane was washed with TBST for 5min for 2 to 3 times until the red staining was completely washed out. Afterwards, blocking was performed with 5% BSA (Sigma-Aldrich Corp., St. Louis, US) in TBST for 1h at room temperature. The incubation of primary antibody lasted overnight at 4°C with simultaneous gentle shaking. The membrane was washed again with TBST for 5min for 3 times, followed by the incubation in secondary antibody for 1h at room temperature with gentle shaking. The information of the used antibodies and the dilution factors are listed in the section

“Primary and secondary antibodies for Western-Blotting” above. After the same washing with TBST again, the membrane was detected with Pierce™ ECL Western Blotting Substrate (1:1 ratio, Thermo Fisher Scientific Inc., Waltham, US) utilizing the Molecular Imager ChemiDoc™ XRS System (Bio-Rad Laboratories, Inc., Hercules, US). The Quantity One program (Bio-Rad Laboratories, Inc., Hercules, US) was used to control the exposure. The first picture was taken at 30s, while the other three were taken at regular intervals between 30s and 20min.

### 3. Results

#### 3.1 *Wnt1* has a strong osteoanabolic impact independent of *Fzd9* in mice

As described in the previous study of our group,<sup>56</sup> the induction of *Wnt1* specifically in osteoblasts had a rapid and marked osteoanabolic function in mice regardless of gender or age, providing a reliable model for the further investigation of the mechanism of *Wnt1* in bone metabolism. Another study of our group revealed that *Fzd9* contributes to maintaining the bone mass by activating bone formation through a noncanonical Wnt-signaling pathway.<sup>60</sup> Since the specific frizzled receptor of *Wnt1* in bone metabolism remains unclear, we crossed the *Wnt1*-transgenic and *Fzd9*-deficient mice to investigate whether *Fzd9* is required for the bone-anabolic function of *Wnt1*.

*Col1a1<sup>tTA</sup>/pTet<sup>Wnt1</sup>/Fzd9<sup>+/+</sup>* and *Col1a1<sup>tTA</sup>/pTet<sup>Wnt1</sup>/Fzd9<sup>-/-</sup>* mice were utilized for analysis, in which doxycycline was either maintained in or removed from the diet for 7 days. The X-ray images showed that the skeletons of all mice are in integrity, without any obvious fractures or malformations (Fig. 1A). Due to the relatively short induction time, the increase of bone mass was not able to be observed on the X-ray. However, through the undecalcified sectioning of lumbar spine and tibia and subsequent von Kossa/van Gieson staining, an obvious phenotype of high bone mass was observed after the removal of doxycycline from the diet for 7 days, in the presence or absence of *Fzd9* (Fig. 1B).

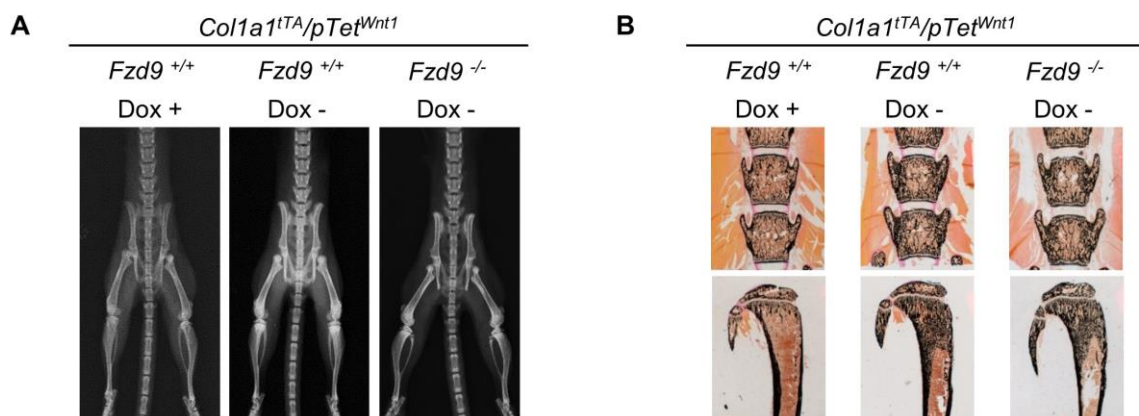


**Figure 1.** *Fzd9* is dispensable for the normal osteoanabolic function of *Wnt1* in mice. (A) Representative X-ray images of *Col1a1<sup>tTA</sup>/pTet<sup>Wnt1</sup>/Fzd9<sup>+/+</sup>* and *Col1a1<sup>tTA</sup>/pTet<sup>Wnt1</sup>/Fzd9<sup>-/-</sup>* 6-week-old female mice. Transgenic *Wnt1*-expression was suppressed by the presence of doxycycline (Dox+) or induced (for 7 days) by the removal of doxycycline (Dox-). (B) Representative undecalcified sections of lumbar spine and tibia of the same mice after von Kossa/van Gieson staining.

Moreover, structural histomorphometry clearly indicated the normal osteoanabolic function of *Wnt1* in the absence of *Fzd9*. In the lumbar vertebral bodies L3 to L4 in *Col1a1<sup>tTA</sup>/pTet<sup>Wnt1</sup>/Fzd9<sup>+/+</sup>* (Dox- for 7 days) and *Col1a1<sup>tTA</sup>/pTet<sup>Wnt1</sup>/Fzd9<sup>-/-</sup>* (Dox- for 7 days) 6-week-old female mice, BV/TV, Tb.N and Tb.Th were all significantly higher than those in the control group (*Col1a1<sup>tTA</sup>/pTet<sup>Wnt1</sup>/Fzd9<sup>+/+</sup>* (Dox+)), while Tb.Sp was significantly lower (Fig. 2A). The same tendencies were observed in the proximal tibial metaphysis of the same mice (Fig. 2B).

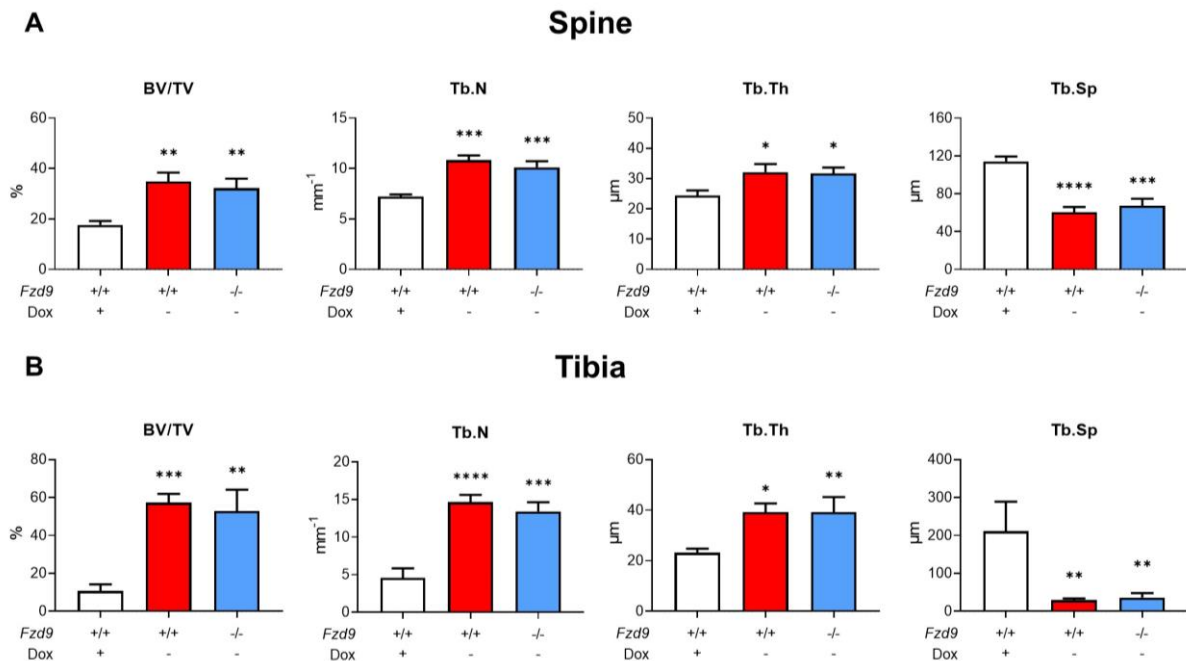


**Figure 2.** Structural histomorphometry confirmed the normal osteoanabolic function of *Wnt1* in the absence of *Fzd9*. (A) Structural parameters of trabecular bone of the lumbar vertebral bodies L3 to L4 of *Col1a1<sup>tTA</sup>/pTet<sup>Wnt1</sup>/Fzd9<sup>+/+</sup>* (Dox+) and *Col1a1<sup>tTA</sup>/pTet<sup>Wnt1</sup>/Fzd9<sup>-/-</sup>* (Dox+ and Dox- for 7 days) 6-week-old female mice, including BV/TV, Tb.N, Tb.Th and Tb.Sp. (B) Structural parameters of trabecular bone in the proximal tibial metaphysis of the same mice. Data were analyzed by two-way ANOVA with Tukey multiple comparisons test (\*  $p < 0.05$ , \*\*  $p < 0.01$ , \*\*\*  $p < 0.001$ , \*\*\*\*  $p < 0.0001$  vs. *Fzd9<sup>+/+</sup>/Dox+* group).  $n = 4$  samples in the *Fzd9<sup>-/-</sup>/Dox-* group,  $n = 3$  in other groups.

In addition, Micro CT analysis was performed to evaluate the impact of *Wnt1* in the femora of mice. The 3D reconstruction of distal femora showed remarkably increased bone mass in *Col1a1<sup>tTA</sup>/pTet<sup>Wnt1</sup>/Fzd9<sup>+/+</sup>* (Dox- for 7 days) and *Col1a1<sup>tTA</sup>/pTet<sup>Wnt1</sup>/Fzd9<sup>-/-</sup>* (Dox- for 7 days) female mice at the age of 6 weeks (Fig. 3A). Here, BV/TV was significantly higher, whereas Tb. TMD was not significantly affected (Fig. 3B). There was no significant difference in Ct. Th in all groups, while Ct. Por was found higher in 6-week-old *Col1a1<sup>tTA</sup>/pTet<sup>Wnt1</sup>/Fzd9<sup>+/+</sup>* (Dox- for 7 days) and *Col1a1<sup>tTA</sup>/pTet<sup>Wnt1</sup>/Fzd9<sup>-/-</sup>* (Dox- for 7 days) female mice (Fig. 3C and 3D).

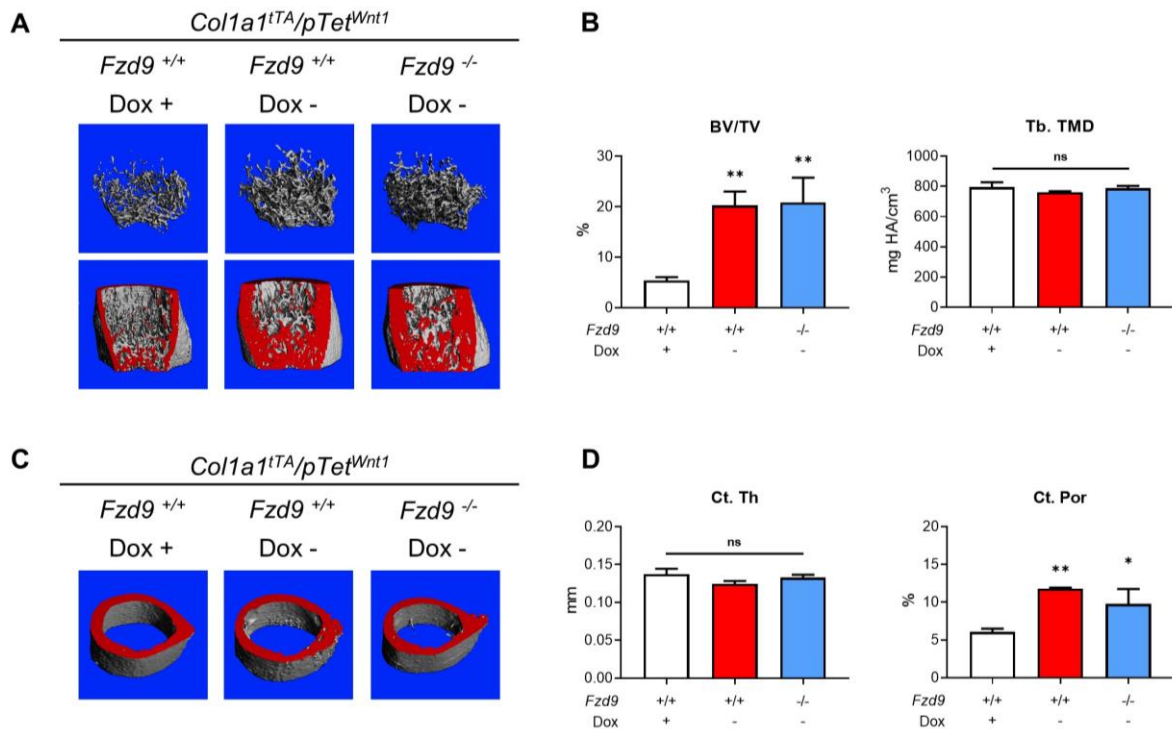


**Figure 3.** Micro CT analysis indicated a strong osteoanabolic impact of *Wnt1* in both trabecular and cortical bone in the femora of mice independent of *Fzd9*. (A) Representative 3D reconstruction images of distal femora (above: segmented trabecular bone, below: cortical and trabecular bone, the vertical cut plane appears red). (B) BV/TV and Tb.TMD from  $\mu$ CT analysis. (C) Representative 3D reconstruction images of cortical bone in the mid-diaphysis of femora from mice with the indicated genotypes and induction status. (D) Ct.Th and Ct.Por as determined by  $\mu$ CT analysis. Data were analyzed by two-way ANOVA with Tukey multiple comparisons test (ns  $p \geq 0.05$ , \*  $p < 0.05$ , \*\*  $p < 0.01$  vs. *Fzd9*<sup>+/+</sup>/Dox+ group). n=4 samples in the *Fzd9*<sup>-/-</sup>/Dox- group. n=3 in other groups.

### 3.2 Bone marrow-derived osteoblasts react to reWnt1/Sfrp1 stimulation via canonical Wnt-signaling in the absence of *Fzd9*

In order to confirm that the osteoanabolic function of *Wnt1* acts independent of *Fzd9*, *in vitro* stimulation with reWnt1/Sfrp1 was performed using bone marrow-derived osteoblasts from wildtype and *Fzd9*<sup>-/-</sup> mice. Stimulation with reWnt1/Sfrp1, reSfrp1 alone, or PBS for 6h was performed after osteogenic differentiation for 5 days or 10 days in wildtype or *Fzd9*-deficient bone marrow-derived osteoblasts, after which expression of *Axin2* and *Apcdd1* was analyzed by qRT-PCR. The expression analysis revealed significant induction of *Axin2* and *Apcdd1* in response to reWnt1/Sfrp1 stimulation in both wildtype and *Fzd9*-deficient mice, indicating that bone marrow-derived osteoblasts can react to reWnt1/Sfrp1 via canonical Wnt-signaling in the absence of *Fzd9* (Fig. 4A and 4B).

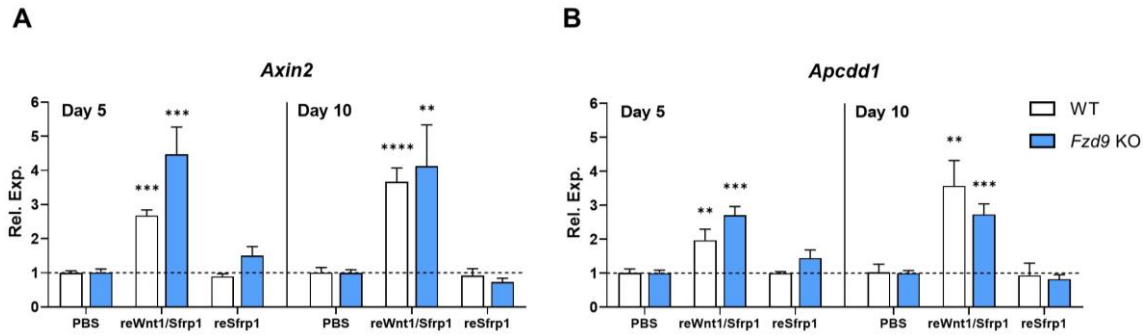


**Figure 4.** Bone marrow-derived osteoblasts can react via canonical Wnt-signaling to the stimulation of reWnt1/Sfrp1 in the absence of *Fzd9*. (A) *Axin2* expression was detected by qRT-PCR in bone marrow-derived osteoblasts from wildtype and *Fzd9*<sup>-/-</sup> mice after osteogenic differentiation of 5 or 10 days followed by 6h stimulation with reWnt1/Sfrp1, reSfrp1 alone, or PBS. (B) *Apcdd1* expression analysis in the same cells. Data were analyzed by one-way ANOVA with Tukey multiple comparisons test (\*\* p<0.01, \*\*\* p<0.001, \*\*\*\* p<0.0001 vs. PBS group). n=3 samples in each group.

### 3.3 reWnt1/Sfrp1 stimulation induced the canonical Wnt-signaling pathway in ST2 cells

Since bone marrow-derived osteoblasts of mice responded to reWnt1/Sfrp1 stimulation significantly at the transcriptional level, we took advantage of the ST2 cell line to further investigate the impact of reWnt1/Sfrp1. ST2 cells were stimulated for 6h with reWnt1/Sfrp1, reSfrp1 alone, or PBS, after which genome-wide expression analysis was performed.

There were thirteen genes induced remarkably with a fold change higher than 5 times in the reWnt1/Sfrp1 group compared to the PBS group, some of which had been identified to be associated with WNT-signaling or bone metabolism (Fig. 5A). More specifically, *Nkd2*, *Apcdd1*, *Ahr* and *Cyr61* are known as the downstream target genes of Wnt-signaling pathway, while *Postn* and *Omd* play important roles in forming extracellular matrix<sup>61-64</sup>. In contrast, all these thirteen genes were not induced in reSfrp1 group except for Gm11096, a predicted gene with unknown function. Based on these data, we hypothesize that ST2 cells respond to reWnt1/Sfrp1 via the canonical Wnt-signaling pathway. Given the strong impact of reWnt1/Sfrp1 on ST2 cells, we additionally checked the expression of common osteogenesis imperfecta (OI) associated genes, yet none of them was significantly affected in both reWnt1/Sfrp1 and reSfrp1 groups (Fig. 5B). Since the specific frizzled receptor of Wnt1 in bone metabolism is still unknown, the expression of all the frizzled receptors (*Fzd1*~*Fzd10*) was analyzed (Fig. 5C). Among all the receptors, *Fzd4* was suppressed most significantly in reWnt1/Sfrp1 group whereas slightly induced in reSfrp1 group,

indicating that Fzd4 is potentially the receptor for Wnt1 in ST2 cells, which would be extremely meaningful to investigate.

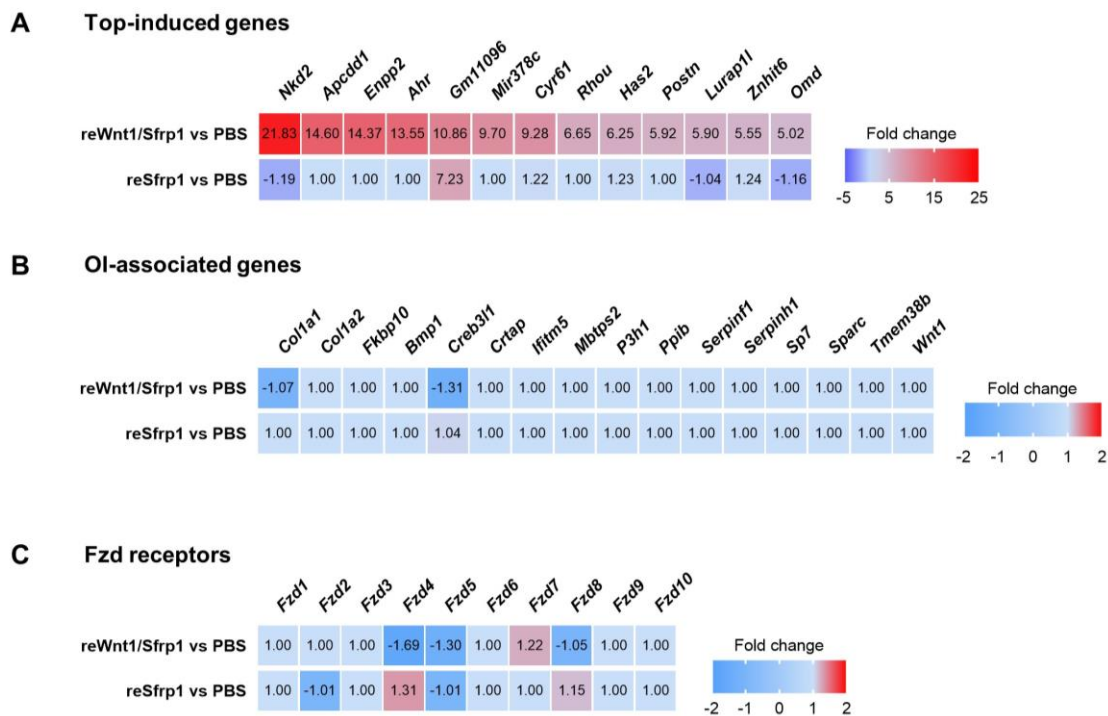


**Figure 5.** Genome-wide expression analysis of ST2 cells treated for 6h with reWnt1/Sfrp1, reSfrp1 alone, or PBS. (A) Genes with a fold change induction higher than 5 times in response to reWnt1/Sfrp1 treatment as compared to PBS. The second line shows the effect of reSfrp1 alone. (B) Regulation of common osteogenesis imperfecta (OI) associated genes in response to reWnt1/Sfrp1 treatment as compared to PBS. The second line shows the effect of reSfrp1 alone. (C) The expression of all frizzled receptors (Fzd1~Fzd10) in response to reWnt1/Sfrp1 treatment as compared to PBS. The second line shows the effect of reSfrp1 alone. Numbers in the boxes indicate the expression fold change.

### 3.4 reWnt1/Sfrp1 significantly induced osteogenic differentiation of ST2 cells

After confirming the impact of reWnt1/Sfrp1 on ST2 cells at transcriptional level, long-term stimulation of ST2 cells with reWnt1/Sfrp1 during osteogenic differentiation was performed to investigate whether reWnt1/Sfrp1 is capable to influence the bone-anabolic process. There was significantly stronger mineralization in reWnt1/Sfrp1 treated groups after 11 or 15 days of continuously stimulation, which was confirmed by Alizarin red staining followed by quantification of mineralization. In contrast, reSfrp1 did not induce the formation of mineralization (Fig. 6A).

On the basis of the previous genome-wide expression analysis, qRT-PCR was performed after the stimulation of 6h to ST2 cells with reWnt1/Sfrp1, reSfrp1 alone, or PBS (Fig. 6B). *Apcdd1* was remarkably induced in the reWnt1/Sfrp1 group, indicating

that reWnt1/Sfrp1 induces canonical Wnt1-signaling in ST2 cells. Importantly, *Omd* and *Postn* were significantly induced after treatment with reWnt1/Sfrp1, which was consistent with the genome-wide expression analysis, revealing the potential downstream mechanism of Wnt1 in osteogenesis. In addition, *Tnfsf11* was suppressed in the reWnt1/Sfrp1 group without reaching significance, while *Tnfrsf11b* was moderately induced. reSfrp1 had consistently no obvious impact on the expression of these target genes.

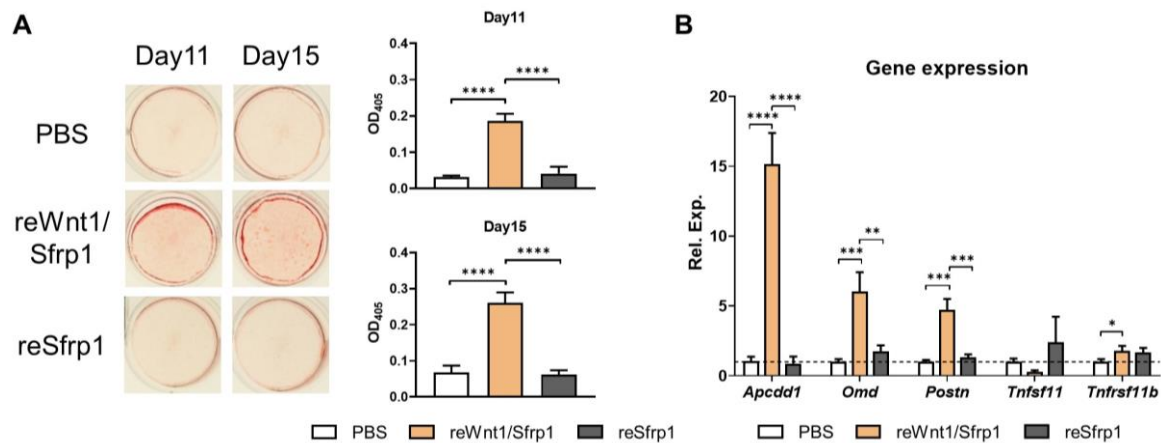


**Figure 6.** reWnt1/Sfrp1 significantly enhanced the osteogenic differentiation of ST2 cells. (A) Representative images of Alizarin red staining of ST2 cells after 11 or 15 days of continuous stimulation with reWnt1/Sfrp1, reSfrp1 alone, or PBS during the osteogenic differentiation process (left), and corresponding quantification of mineralization (right). (B) qRT-PCR gene expression analysis in ST2 cells after 6h stimulation with reWnt1/Sfrp1, reSfrp1 alone, or PBS, indicating an activation of canonical Wnt-signaling and potential downstream targets with the significant induction of *Apcdd1*, *Omd* and *Postn*. Data were analyzed by one-way ANOVA with Tukey multiple comparisons test (\*  $p < 0.05$ , \*\*  $p < 0.01$ , \*\*\*  $p < 0.001$ , \*\*\*\*  $p < 0.0001$ ).  $n = 3$  samples in each group.

### 3.5 *Omd* and *Postn* were not consistently induced in long bone and calvaria of *Wnt1*-transgenic mice

The expression analysis of ST2 cells stimulated with reWnt1/Sfrp1 provided very valuable information for investigating the downstream mechanism of Wnt1 in bone metabolism. We took advantage of the *Wnt1*-transgenic mice to investigate if *Omd* and *Postn* could be induced by the induction of *Wnt1* *in vivo*.

qRT-PCR was performed to analyze the expression of *Omd* and *Postn* in long bones (femora and tibiae) and calvariae. Male *Col1a1<sup>tTA</sup>/pTet<sup>Wnt1</sup>* mice of 6 weeks of age were utilized for analysis. Transgenic *Wnt1* was induced by removing doxycycline from the diet for 2 days while in the controls the transgene was repressed by maintaining doxycycline in the diet. *Omd* was induced significantly in long bones when transgenic *Wnt1* was induced by the removal of doxycycline (Fig. 7A). However, in calvaria *Omd*

was not affected by the induction of transgenic *Wnt1* (Fig. 7B). As for the expression of *Postn*, there was no significant difference, regardless of the bone site or the condition of transgenic *Wnt1* (Fig. 7A and B). This inconsistency again raised the question about the exact downstream mechanism of Wnt1 in bone metabolism.

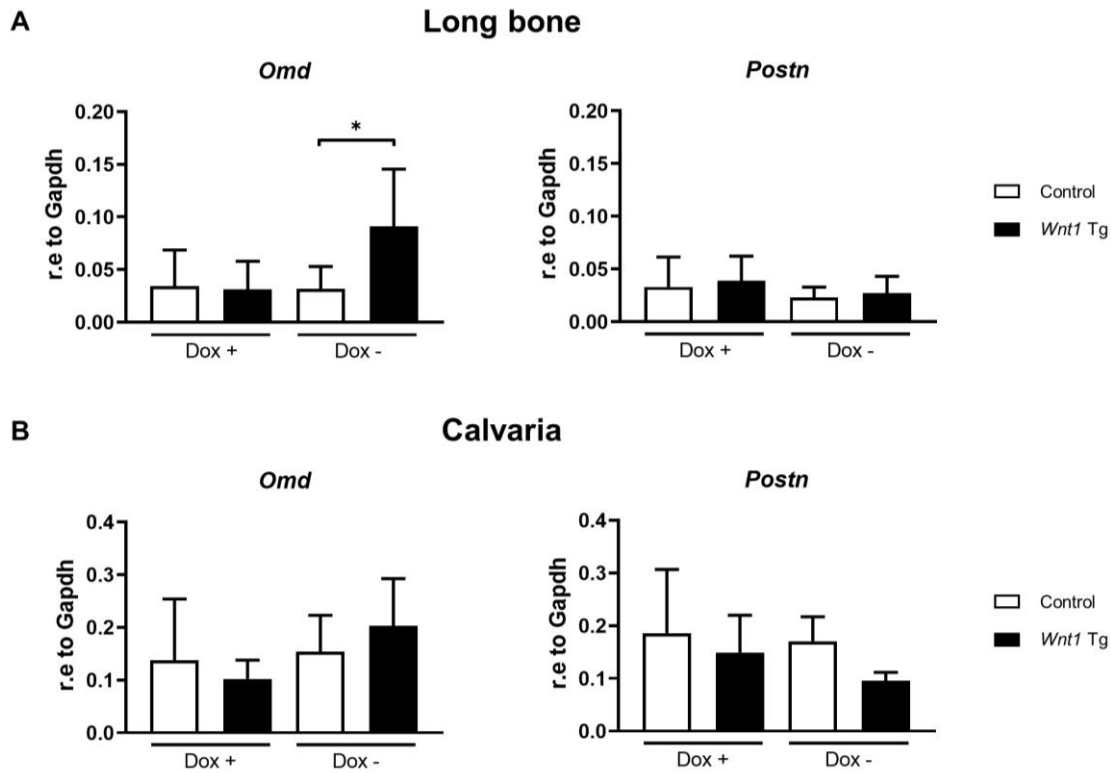


**Figure 7.** *Omd* and *Postn* was not enhanced consistently by the induction of transgenic *Wnt1* expression *in vivo*. (A) *Omd* and *Postn* expression was detected by qRT-PCR, utilizing long bones (femora and tibiae) from *Col1a1<sup>tTA</sup>/pTet<sup>Wnt1</sup>* male 6-week-old mice, in which transgenic *Wnt1* expression was repressed by doxycycline (Dox+) or induced (for 2 days) by the removal of doxycycline (Dox-) from the diet. (B) Expression analysis in calvariae from mice treated in the same way as above. Data were analyzed by two-way ANOVA with Tukey multiple comparisons test (\*  $p < 0.05$ ).  $n = 5$  and  $3$  samples in Dox+ control and *Wnt1* Tg groups respectively.  $n = 7$  and  $6$  samples in Dox- control and *Wnt1* Tg groups respectively.

### 3.6 A pathogenic *Wnt1* mutation (G177C) impairs the impact of *Wnt1* *in vitro*

In order to further investigate the mechanism of *Wnt1* in bone metabolism, we took advantage of wildtype and mutant *Wnt1* expression plasmids to perform transfection in ST2 cells. The mutant *WNT1* (G177C) was previously reported to cause osteogenesis imperfecta type XV (OI-XV) in humans.<sup>59</sup>

After stable transfection with an empty vector (pLNCX), the wildtype *Wnt1* expression plasmid (*Wnt1*), or the *Wnt1-G177C* expression plasmid (*Wnt1-G177C*), ST2 cells underwent osteogenic differentiation for 15 days. Subsequently, Alizarin red staining was performed, followed by quantification of mineralization. The wildtype *Wnt1* expression plasmid remarkably promoted the formation of mineralized matrix during osteogenic differentiation, whereas the mutant *Wnt1* plasmid did not affect the formation of bone nodules significantly (Fig. 8A). Furthermore, gene expression of ST2 cells was analyzed by qRT-PCR after transient transfection with the same plasmids followed by 5 days of osteogenic differentiation. The significantly higher expression of *Wnt1* in the *Wnt1* and the *Wnt1-G177C* groups confirmed the efficiency of the transfection. Important genes that are associated with bone anabolism, including *Alpl*, *Bglap* and *Ibsp*, were significantly induced in the *Wnt1* group, demonstrating the strong impact of *Wnt1* on bone anabolism (Fig. 8B). Consistently with the ST2 cells in re*Wnt1*/Sfrp1 stimulation, *Apcdd1*, *Omd* and *Postn* were significantly induced by *Wnt1* (Fig. 8C), indicating the potential downstream mechanism of *Wnt1* in bone metabolism. Importantly, none of these Wnt target genes was induced with the *Wnt1* expression plasmid containing the G177C mutation.

Based on the potential downstream mechanism, we utilized the mouse line carrying the *Wnt1-G177C* mutation. Protein extracts were obtained from the femora and tibiae of a male 38-week-old mouse and a matched control. Extractions of trabecular and cortical bone were prepared separately, followed by Western-Blotting and corresponding Ponceau S staining. Although the bands of *Col1a1* did not appear in the expected molecular weight range, a difference of *Omd* expression was observed between wildtype and *Wnt1-G177C* mice, especially in cortical bone with corresponding Ponceau S staining as a loading control (Fig. 8D). However, the exact mechanism certainly remains to be further investigated and verified.

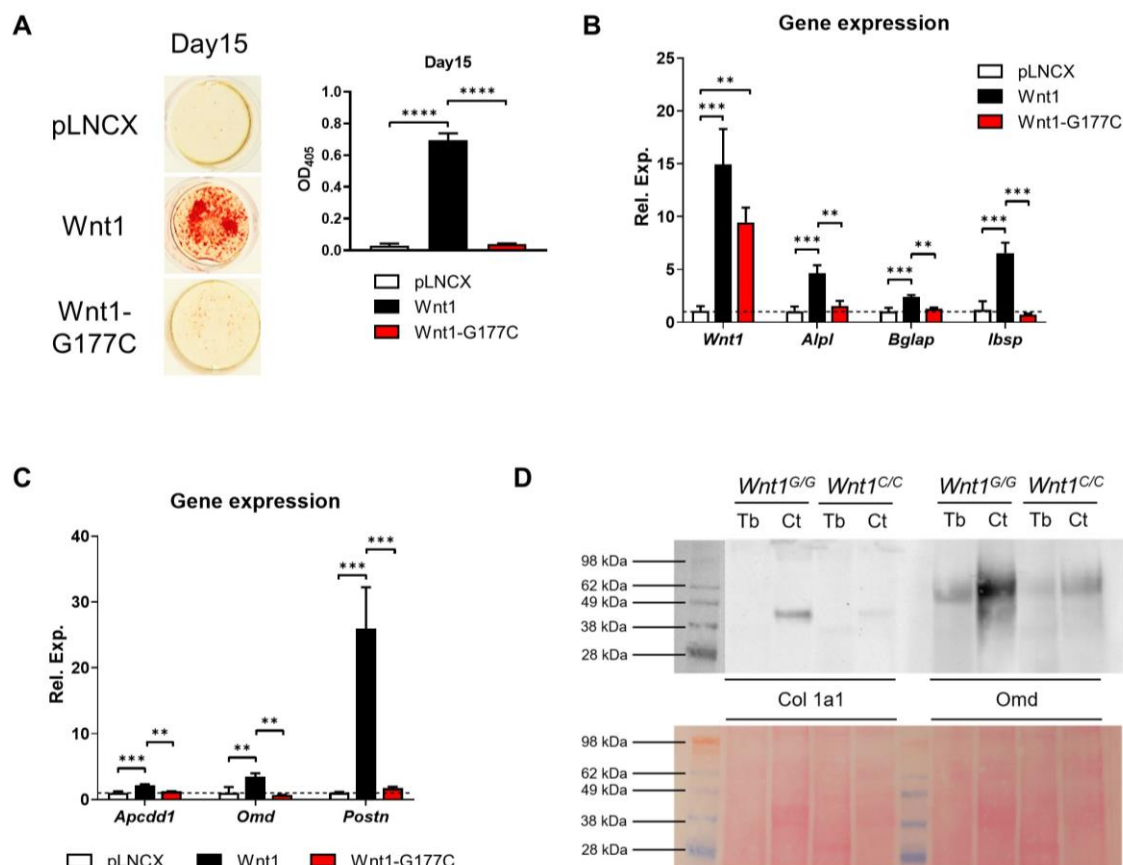


**Figure 8.** *Wnt1* significantly mediated osteogenic differentiation *in vitro*, while the mutant *Wnt1* (*G177C*) showed no comparable effect. (A) Representative images of Alizarin Red staining of ST2 cells which were stably transfected with empty vector (pLNCX) or with one of the expression plasmids (wildtype: *Wnt1* / mutant *Wnt1*: *Wnt1-G177C*) and underwent osteogenic differentiation of 15 days (left). Corresponding quantification of mineralization was shown on the right. (B) and (C) Expression analysis of indicated genes by qRT-PCR in ST2 cells after osteogenic differentiation of 5 days since transiently transfected with the same plasmids. Data were analyzed by one-way ANOVA with Tukey multiple comparisons test (\*\*  $p < 0.01$ , \*\*\*  $p < 0.001$ , \*\*\*\*  $p < 0.0001$ ).  $N = 3$  samples in each group. (D) A preliminary analysis of *Col1a1* and *Omd* expression by Western-Blotting and corresponding Ponceau S staining in trabecular bone (Tb) and cortical bone (Ct) of femora and tibiae in male 38-week-old *Wnt1<sup>G/G</sup>* (*Wnt1<sup>+/+</sup>*) and *Wnt1<sup>C/C</sup>* (*Wnt1<sup>G177C/G177C</sup>*) mice.  $n = 1$  sample in each group.

### 3.7 Stimulation of calvarial or bone marrow-derived osteoblasts with reWnt1/Sfrp1 did not increase *Postn/Omd* expression or osteogenesis

To further investigate the impact of *Wnt1* to osteoblasts in different stages in osteogenic differentiation, we isolated calvarial osteoblasts from wildtype mice for the stimulation with reWnt1/Sfrp1. Gene expression analysis by qRT-PCR was performed after 6h of stimulation with reWnt1/Sfrp1, reSfrp1 alone, or PBS before starting osteogenic differentiation or on day 5, 10, 15 and 20 of osteogenic differentiation

respectively. The stimulation with reWnt1/Sfrp1 significantly induced *Axin2* and *Apcdd1* at all the time points, while reSfrp1 alone did not affect the expression of these genes, indicating the activation of the canonical Wnt-signaling pathway, which is consistent with the results observed in ST2 cells. However, *Omd* and *Postn* were not induced by reWnt1/Sfrp1. In addition, genes that are commonly associated with bone metabolism were analyzed, including *Ccnd1*, *Runx2*, *Tnfsf11*, *Sp7* and *Col1a1*. However, among these only few were modulated inconsistently and moderately by reWnt1/Sfrp1 or reSfrp1 stimulation at different time points (Fig. 9A to E). In accordance with the stimulation of ST2 cells, long-term continuous stimulation for 15 days during osteogenic differentiation with reWnt1/Sfrp1, reSfrp1 alone, or PBS was applied to calvarial osteoblasts. However, the outcome was opposing the previous results from the experiments with ST2 cells, since reWnt1/Sfrp1 did not induce osteogenesis, which was confirmed by Alizarin red staining followed by quantification of mineralization (Fig. 9F).

Collectively, calvarial osteoblasts of mice were able to respond to reWnt1/Sfrp1 via canonical Wnt-signaling pathway. However, the cells displayed vastly different characteristics with regard to *Omd* and *Postn* expression as well as osteogenesis in response to reWnt1/Sfrp1 stimulation as compared to ST2 cells that were treated with reWnt1/Sfrp1 or transfected with the *Wnt1* expression plasmid.

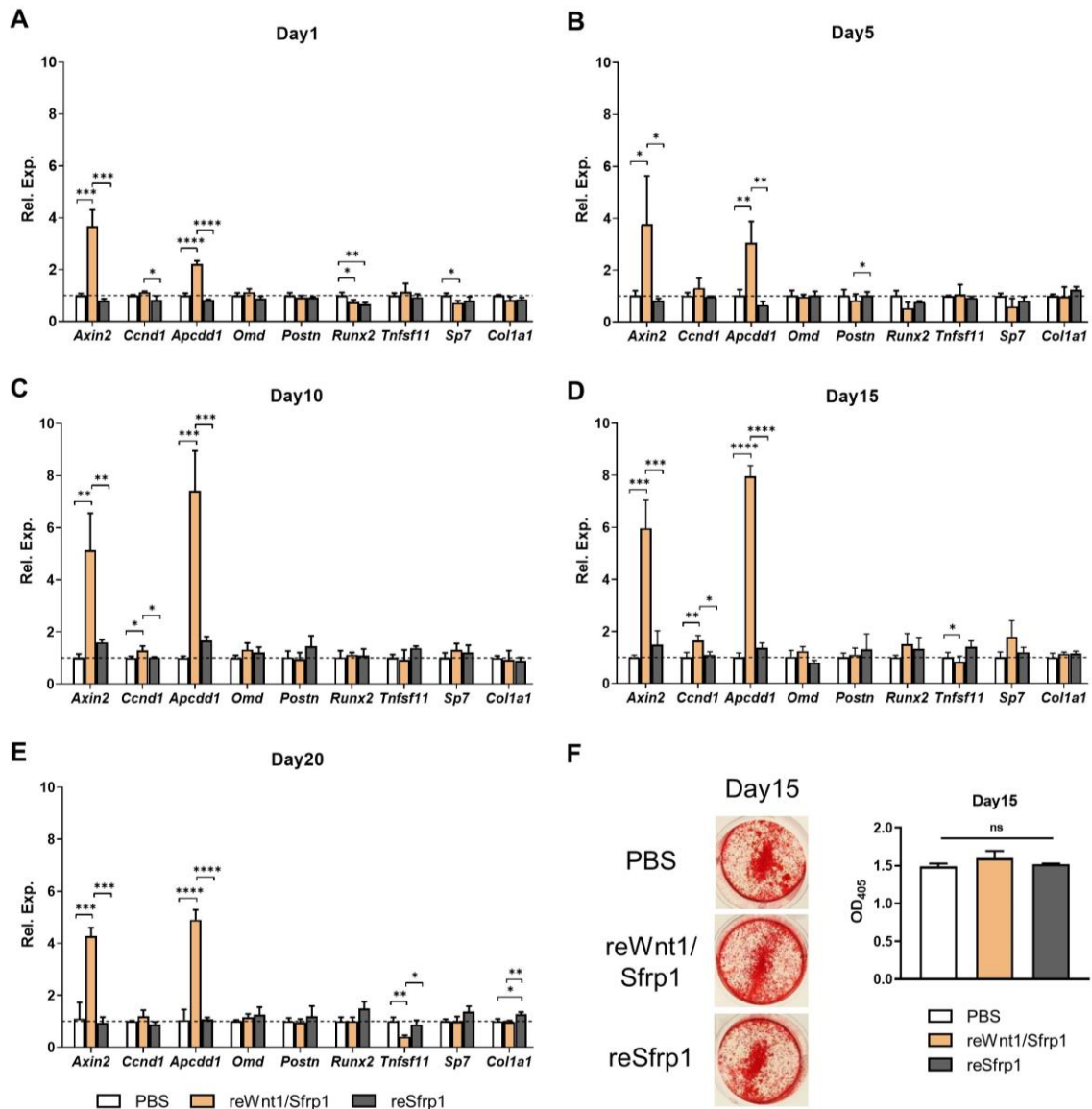


**Figure 9.** Short-term (6h) stimulation of reWnt1/Sfrp1 in calvarial osteoblasts in wildtype mice transcriptionally indicated an activation of canonical Wnt-signaling, while long-term (15 days) continuous stimulation during osteogenic differentiation showed no obvious induction of osteogenesis. (A) Expression analysis of indicated genes by qRT-PCR in calvarial osteoblasts in wildtype mice after 6h stimulation with reWnt1/Sfrp1, reSfrp1 alone, or PBS (marked as Day1). (B) ~ (E) Expression analysis after the same 6h stimulation on day 5, 10, 15 and 20 of osteogenic differentiation. (F) Representative images of Alizarin Red staining of calvarial osteoblasts from wildtype mice after 15 days of continuous stimulation with reWnt1/Sfrp1, reSfrp1 alone, or PBS during osteogenic differentiation (left). Corresponding mineralization quantification was shown on the right. Data were analyzed by one-way ANOVA with Tukey multiple comparisons test (ns  $p \geq 0.05$ , \*  $p < 0.05$ , \*\*  $p < 0.01$ , \*\*\*  $p < 0.001$ , \*\*\*\*  $p < 0.0001$  vs. PBS group).  $n=3$  samples in each group.

Given that calvarial osteoblasts are distinctly different from osteoblasts that distribute in long bones and spines, we took advantage of bone marrow-derived osteoblasts from femora and tibiae of wildtype mice to investigate the impact of reWnt1/Sfrp1.

The same short-term stimulation of 6h with reWnt1/Sfrp1, reSfrp1 alone, or PBS was performed at the same time points in osteogenesis differentiation, as well as the long-term continuous stimulation of 15 days. Besides, qRT-PCR, Alizarin red staining and quantification of mineralization were also performed as indicated above. Consistently, *Axin2* and *Apcdd1* were induced significantly by short-term stimulation with reWnt1/Sfrp1. In contrast, reSfrp1 alone was not able to affect the expression of *Axin2* and *Apcdd1*. *Omd* was only slightly induced by reWnt1/Sfrp1 on day1, 10 and 20, while *Postn* was not significantly affected at any time point (Fig.10A to E). Although the overall osteogenesis after 15 days of differentiation with continuous treatment was much stronger than that of calvarial osteoblasts indicated above, the quantification of mineralization demonstrated no obvious effect of reWnt1/Sfrp1 on osteogenesis (Fig.10F).

Based on these current data, we conclude that calvarial and bone marrow-derived osteoblasts are able to react to reWnt1/Sfrp1 via the canonical Wnt-signaling pathway. However, the regulation of downstream target genes by reWnt1/Sfrp1 remains to be further investigated. Moreover, the fact that long-term reWnt1/Sfrp1 stimulation to calvarial and bone marrow-derived osteoblasts did not contribute to osteogenesis is surprising.

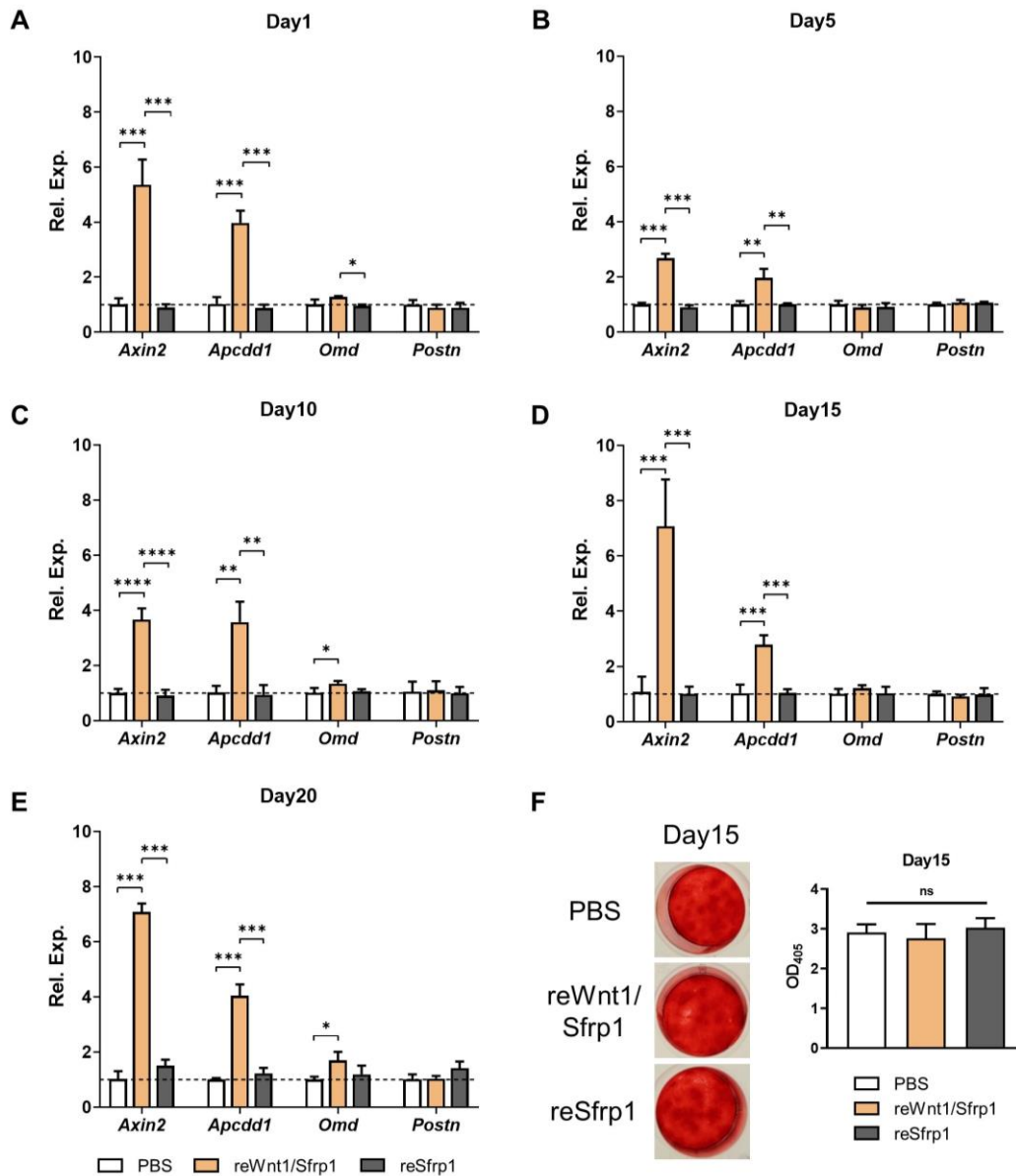


**Figure 10.** Short-term (6h) stimulation of reWnt1/Sfrp1 in bone marrow-derived osteoblasts in wildtype mice indicated that canonical Wnt-signaling pathway was activated at transcription level, while there was no significant induction of osteogenesis after continuous long-term (15 days) stimulation. (A) ~ (E) Expression analysis of indicated genes by qRT-PCR in bone marrow-derived osteoblasts in wildtype mice after 6h stimulation with reWnt1/Sfrp1, reSfrp1 alone, or PBS at day 0, 5, 10, 15 and 20 of osteogenic differentiation (F) Representative images of Alizarin Red staining and corresponding quantification of mineralization after long-term (15 days) stimulation with reWnt1/Sfrp1, reSfrp1 alone, or PBS during osteogenic differentiation. Data were analyzed by one-way ANOVA with Tukey multiple comparisons test (ns  $p \geq 0.05$ , \*  $p < 0.05$ , \*\*  $p < 0.01$ , \*\*\*  $p < 0.001$ , \*\*\*\*  $p < 0.0001$ ).  $n = 3$  samples in each group.

### **3.8 The differential responses of ST2 and MC3T3 cells towards reWnt1/Sfrp1 stimulation may be related to differential expression of putative Wnt1 receptors**

Since unraveling the downstream mechanism and the receptor of Wnt1 in bone metabolism are the most important goals in this context, we also applied similar reWnt1/Sfrp1 stimulation to MC3T3 cells for further investigation. Of note, MC3T3 reacted to the stimulation of reWnt1/Sfrp1 differently from ST2 cells, calvarial and bone marrow-derived osteoblasts. The mineralization was significantly less after osteogenic differentiation for 15 days accompanied by continuous treatment of reWnt1/Sfrp1 compared with PBS, while reSfrp1 alone did not affect the osteogenesis significantly (Fig 11A). With respect to gene expression following short-term stimulation for 6h, *Axin2* was significantly but moderately induced in the reWnt1/Sfrp1 group, whereas *Apcdd1* was not affected in all three groups. Partially consistent with ST2 cells, *Omd* was significantly induced by reWnt1/Sfrp1 treatment, however, there was only a tendency for *Postn* induction (Fig 11B).

As a calvaria-derived osteoblastic cell line, MC3T3 possibly possesses different characteristics in osteogenesis when compared with the mesenchymal progenitor cell line ST2. This provided a new starting point for the further investigation of the putative Wnt1 receptor. Therefore, the expression of all the Lrp and Fzd receptors was analyzed by qRT-PCR in ST2 and MC3T3 cells (Fig. 11C). Surprisingly, the expression of most receptors is quite different in these two cell lines. Most importantly, the expression of *Lrp5*, *Fzd2*, *Fzd4*, *Fzd8* was significantly higher in ST2 cells compared to MC3T3 cells, indicating that these receptors could be potential factors which caused the different response patterns to reWnt1/Sfrp1 in ST2 and MC3T3 cells.

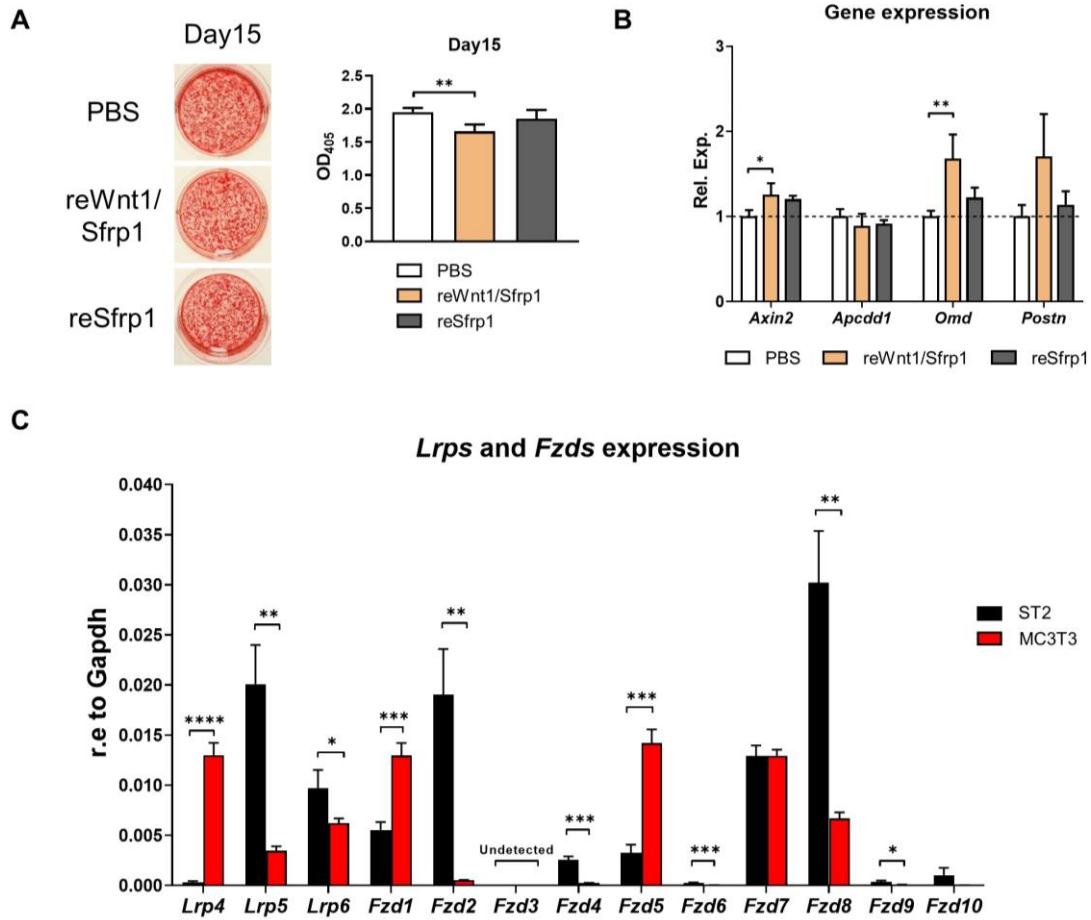


**Figure 11.** MC3T3 cells responded to either short-term (6h) or long-term (15 days) stimulation of reWnt1/Sfrp1 differently compared to ST2 cells, calvarial and bone marrow-derived osteoblasts. (A) Representative images of Alizarin Red staining and mineralization quantification of MC3T3 cells after continuously stimulated by reWnt1/Sfrp1, reSfrp1 alone, or PBS for 15 days during osteogenic differentiation. (B) Gene expression was analyzed by qRT-PCR in MC3T3 cells after stimulation for 6h. Data were analyzed by one-way ANOVA with Tukey multiple comparisons test (\*  $p < 0.05$ , \*\*  $p < 0.01$ ).  $N = 3$  samples in each group. (C) Comparison of the expression of indicated *Lrps* and *Fzds* in ST2 and MC3T3 cells by qRT-PCR. Data were analyzed by unpaired t-test (\*  $p < 0.05$ , \*\*  $p < 0.01$ , \*\*\*  $p < 0.001$ , \*\*\*\*  $p < 0.0001$ ).  $n = 3$  samples in each group.

## 4. Discussion

Bone modeling and bone remodeling are essential physiological processes in humans, which coordinate with each other as well as with a series of other metabolic processes. This dynamic balance ensures normal skeletal development and bone turnover.<sup>12</sup> As a crucial regulator of biological metabolism, WNT-signaling has been established by numerous studies to be closely linked with bone homeostasis and diseases.<sup>37</sup> Some mutations of WNT-signaling components have been identified to be associated with disorders of bone homeostasis, causing either low bone mass or high bone mass diseases, such as osteoporosis-pseudoglioma syndrome (OPPG) and Van Buchem disease (VBD) that are caused by mutations of LRP5 or Sclerostin respectively.<sup>4,65,66</sup>

In previous studies, *Wnt1* was found to be a crucial factor for the development of the central nervous system during the embryogenic stage in mice. *Wnt1*-deficiency causes severe defects in the brain structure and consequently early postnatal lethality.<sup>67,68</sup> A brain phenotype was also observed in the *swaying* mice, which carry an inactivating mutation of *Wnt1*, shortly after the publication of the *Wnt1*-deficient mouse model.<sup>69</sup> Interestingly, several years later, after first indications of the role of WNT1 in human skeletal metabolism were published, the *swaying* mice were reported to additionally display an obvious phenotype of osteogenesis imperfecta (OI).<sup>70</sup> Meanwhile, many clinical studies demonstrated that WNT1 plays a key role in the maintenance of bone integrity. Inactivating mutations of *WNT1* were identified to cause either early-onset osteoporosis (EOOP) or osteogenesis imperfecta (OI) in patients.<sup>8,58,59,71</sup> On the contrary, induction of *Wnt1* in osteoblasts leads to a contrasting and remarkable osteoanabolic response in mice, as demonstrated in the previous study of our group.<sup>56</sup> Hence, WNT1 was identified to be closely associated with bone metabolism. Therefore, it is meaningful to investigate the mechanism of WNT1 in bone metabolism, which could potentially provide new concepts for the therapy of metabolic bone disorders and skeletal diseases associated with impaired WNT-signaling.

Previous studies of our group revealed that a R235W mutation of *Wnt1* in mice results in a bone-specific early-onset osteoporotic phenotype similar to the symptoms observed in the respective patients,<sup>72</sup> whereas the osteoblast-specific inducible *Wnt1* expression causes rapid and significant osteogenesis in mice independent of *Lrp5*.<sup>56</sup> Furthermore, in another study of our group it was demonstrated that *Fzd9* plays a role in activation of bone formation through the noncanonical Wnt-signaling pathway. Most importantly, *Fzd9*-deficient mice display a phenotype with low bone mass due to the impaired bone formation.<sup>60</sup> In this thesis, I was aiming to further investigate the mechanism of WNT1 in the regulation of bone metabolism.

Given the impact of *Fzd9* in bone anabolism, we hypothesized that *Fzd9* is potentially a relevant receptor of *Wnt1* in osteoblasts. By crossing the osteoblast-specific inducible *Wnt1*Tg mice with the *Fzd9*-deficient mice, we investigated if *Fzd9* is required for the osteogenic function of *Wnt1*. The *Col1a1<sup>tTA</sup>/pTet<sup>Wnt1</sup>/Fzd9<sup>-/-</sup>* mice responded rapidly and significantly to the *Wnt1* induction after the removal of doxycycline from

diet comparable to *Col1a1<sup>tTA</sup>/pTet<sup>Wnt1</sup>/Fzd9<sup>+/+</sup>* mice, displaying high bone mass especially in trabecular bone. Furthermore, the induction of *Axin2* and *Apcdd1* in bone marrow-derived osteoblasts in response to reWnt1/Sfrp1 treatment confirmed *in vitro* that canonical Wnt-signaling was induced in the absence of Fzd9. These results indicate that the strong osteoanabolic response to Wnt1 is independent of Fzd9. However, ten different frizzled receptors have been identified so far and whether any of the others could be in compensation for the deficiency of Fzd9 remains unclear and needs to be further investigated. The functional mode of LRP5 and LRP6 is an informative example as these two co-receptors possess similar and redundant functions in the WNT-signaling pathway.<sup>73</sup>

In order to investigate the mechanism of WNT1 in the osteoanabolic process, genome-wide expression analysis was performed with ST2 cells which were stimulated with reWnt1/Sfrp1, reSfrp1 alone, or PBS for 6h. Among the genes with a fold-change induction higher than 5 times, *Nkd2*, *Apcdd1*, *Enpp2*, *Ahr*, *Cyr61*, *Postn* have been reported to be associated with Wnt-signaling.<sup>62,74-78</sup> In contrast, reSfrp1 alone didn't induce any of these genes. Moreover, it was reported that deficiency of *Postn* in mice significantly influences bone material properties and impairs local remodeling processes in response to fatigue, thus affecting damage accumulation and the repair of bone.<sup>79</sup> *Postn* was also shown to play an important role in bone homeostasis, particularly in the remodeling response to mechanical loading in cortical bone.<sup>80,81</sup> *Omd* was more than 5-fold induced by reWnt1/Sfrp1 compared with PBS, whereas not induced by reSfrp1 alone. *Omd* was revealed to be able to reduce the fibril diameter and variability of type-I collagen basically via weak electrostatic forces.<sup>82,83</sup> Moreover, previous studies indicated that *Omd* contributes to the differentiation and maturation of osteoblasts *in vitro*, whereas, the mechanism of *Omd* in the mineralization process *in vivo* remains unclear.<sup>84,85</sup> Since an *Omd*-deficient mouse model has not been analyzed so far for skeletal defects, future studies are needed to analyze the role of *Omd* *in vivo*. In summary, reWnt1/Sfrp1 has a strong impact on gene expression of ST2 cells, particularly involving the Wnt-signaling pathway.

Considering that mutations of WNT1 can cause osteogenesis imperfecta (OI) in humans, we also screened all common OI-associated genes in the genome-wide expression analysis. However, all the OI-associated genes were not significantly regulated by reWnt1/Sfrp1 in ST2 cells. Since exploring the receptor of WNT1 in bone metabolism is one of the goals of this study, we also focused on the expression of all Frizzled receptors. Interestingly, *Fzd4* was suppressed most strongly by reWnt1/Sfrp1 with a fold-change of 1.69. During the functioning of signaling pathways, negative feedback is an important mechanism of regulation, including the downregulation of receptor gene expression. For example, estrogen participates in self-regulation through the mediation of the expression of its own receptors.<sup>86</sup> Based on this theory, *Fzd4* is potentially a receptor of Wnt1 in ST2 cells. Of note, it was demonstrated that osteoblast-specific deficiency of *Fzd4* results in reduced cortical tissue mineral density and impaired mineralization process with consequent reduced trabecular bone mass in femora.<sup>87</sup> Moreover, *Fzd4* possibly displays overlapping functions with *Fzd8*.<sup>87</sup>

Therefore, it is highly worthwhile to take Fzd4 and Fzd8 into consideration as potential receptors of Wnt1 in future studies.

To further investigate the impact of Wnt1 in osteogenesis, we took advantage of the ST2 cell line for the stimulation with reWnt1/Sfrp1. The Alizarin red staining and corresponding quantification of mineralization indicated that reWnt1/Sfrp1 significantly facilitated the mineralization of ST2 cells during osteogenic differentiation. In qRT-PCR analysis, the significant induction of *Apcdd1* showed that canonical Wnt-signaling was induced by reWnt1/Sfrp1 stimulation. Furthermore, *Omd* and *Postn* were significantly induced by reWnt1/Sfrp1, which is consistent with the genome-wide expression analysis, indicating the potential downstream mechanism of Wnt1 in ST2 cells. To verify the role of *Omd* and *Postn* in the downstream mechanism of WNT-signaling, we utilized the *Col1a1<sup>tTA</sup>/pTet<sup>Wnt1</sup>* mice for the induction of *Wnt1 in vivo*. However, *Omd* and *Postn* were not induced consistently in the long bone and calvaria of mice after the induction of *Wnt1* for 2 days. Only in long bones (femora and tibiae) of *Wnt1*-induced mice, *Omd* expression was significantly increased. One possible explanation of this is that the induction of *Wnt1 in vivo* has different effects with regard to the downstream target genes in long bones and calvaria, but the exact role of *Omd* and *Postn* in the downstream mechanism of WNT-signaling remains to be further investigated.

We also performed transfection of ST2 cells to investigate the impact of Wnt1. In addition to the wildtype Wnt1 expression plasmids, we utilized the Wnt1-G177C expression plasmid, which contains the mutation p.Gly177Cys, where the highly conserved glycine at position 177 is substituted by cysteine, causing osteogenesis imperfecta XV (OI-XV) in humans and mice.<sup>59</sup> Alizarin red staining and corresponding quantification of mineralization revealed a strongly increased production of mineralized matrix induced by wildtype *Wnt1* during osteogenic differentiation. In contrast, the Wnt1-G177C mutation did not induce mineralization in ST2 cells. Moreover, the significant increase of *Alpl*, *Bglap* and *Ibsp* expression indicated that *Wnt1* greatly induced the bone formation process, whereas the mutant *Wnt1* did not. Consistently with the previous experiments, *Apcdd1*, as well as *Omd* and *Postn*, were significantly induced by *Wnt1*, which again drew our attention to the question whether *Omd* and *Postn* play important roles in the downstream mechanism of WNT1-signaling in the skeletons. Since we observed decreased bone mass and spontaneous fractures in mice homozygous for the Wnt1-G177C mutation in a related project, we performed Western-blotting of protein extracts from trabecular and cortical femora and tibiae from a *Wnt1<sup>G177C/G177C</sup>* mouse. Although *Col1a1* was not detected perfectly, the result provided a preliminary indication that the *Omd* content in cortical bone is higher, and the mutant mouse has less *Omd* in cortical bone. This could be a possible reason for the reduced bone material quality and osteogenesis imperfecta phenotype caused by the Wnt1-G177C mutation. Certainly, these are very preliminary results and more samples are needed to get unbiased and reliable data. Therefore, performing more Western-blotting of bone protein extracts is another important task in our future studies.

Since ST2 cells might have different biological properties during osteogenic differentiation compared with primary osteoblasts, we isolated primary calvarial osteoblasts and bone marrow-derived osteoblasts from wildtype mice to repeat the stimulation with reWnt1/Sfrp1 after osteogenic differentiation. In line with ST2 cells, *Axin2* and *Apcdd1* expression levels were significantly increased in both types of osteoblasts at different time points after the stimulation with reWnt1/Sfrp1, indicating the induction of canonical Wnt-signaling. However, *Postn* was not induced at any of the time point in both osteoblasts by reWnt1/Sfrp1. Although *Omd* expression was significantly but only slightly increased at some of the evaluated time points in bone marrow-derived osteoblasts, this result was in stark contrast to the tendencies indicated by the previous experiments. Besides, it was surprising that the continuous administration of reWnt1/Sfrp1 did not enhance the mineralization in both osteoblasts during osteogenic differentiation.

Additionally, we took advantage of MC3T3 cells to perform the reWnt1/Sfrp1 stimulation. Interestingly, MC3T3 cells responded to reWnt1/Sfrp1 stimulation differently to all previously investigated cell types. Long-term stimulation with reWnt1/Sfrp1 during osteogenic differentiation slightly but significantly suppressed the mineralization of MC3T3 cells. *Axin2* was slightly but significantly induced by reWnt1/Sfrp1, whereas *Apcdd1* was not. *Omd* and *Postn* were induced by reWnt1/Sfrp1 after 6h stimulation, with only *Omd* expression reaching statistical significance. As a pre-osteoblastic cell line, MC3T3 cells are more similar to osteoblasts than ST2 cells, thus potentially explaining the closer resemblance of the data obtained from MC3T3 cells to the results from primary osteoblasts. We screened the expression of and *Lrp4/5/6* and all the frizzled receptors in ST2 and MC3T3 cells. Interestingly, we found remarkable differential expression of those receptors in ST2 and MC3T3 cells. Of note, *Lrp5*, *Fzd2*, *Fzd4*, *Fzd8* were expressed significantly higher in ST2 cells than in MC3T3 cells, indicating that these receptors are possibly mediating the observed response of ST2 cells to reWnt1/Sfrp1 that was lacking in MC3T3 cells. Previous studies from our lab demonstrated that the function of Wnt1 in bone anabolism is independent of *Lrp5* in mice,<sup>56</sup> and *Fzd8*-deficient mice only display osteopenia with normal bone formation.<sup>88</sup> There is currently no literature available focusing on the interaction of *Fzd2* with Wnt1. However, *Fzd4* was significantly and strongly suppressed by reWnt1/Sfrp1 in ST2 cells as discussed above, additionally, there is evidence that *Fzd4* can influence skeletal metabolism.<sup>87</sup> Therefore, we hypothesize that *Fzd4* is potentially a receptor for Wnt1 in ST2 cells. This will be an important hypothesis to be addressed in future research.

In summary, WNT1 plays a very important role in bone metabolism and contributes to the maintenance of the skeletal integrity. Inactivating mutations of *WNT1* cause EOOP or OI in humans. The activation of *Wnt1* in mice leads to a rapid and markable increase in bone mass, which is independent of *Lrp5* or *Fzd9*. ST2 cells respond to reWnt1/Sfrp1 by enhanced mineralization during osteogenic differentiation as well as by expression of genes involved with canonical Wnt-signaling. However, primary calvarial and bone marrow-derived osteoblasts as well as MC3T3 cells did not show the same response

to reWnt1/Sfrp1 with regard to mineralization and gene expression. Based on these differences described in the current results, we have identified Fzd4 as a potential receptor candidate for Wnt1. The results from this thesis implicate Omd and Postn as potential downstream targets that mediate the influence of Wnt1 on skeletal integrity. However, further research is required to substantiate this hypothesis.

## 5. Summary

The ligand WNT1 has been proved to be crucial for skeletal integrity and metabolism in humans. Indeed, there are many patients suffering from skeletal diseases which are caused by mutations of WNT1, including early-onset osteoporosis (EOOP) and osteogenesis imperfecta (OI). Although the actual metabolic conditions of humans and mice are quite different, investigating the metabolism by utilizing mouse models is the first step to reveal the mechanism of those diseases and metabolic activities. The activation of Wnt1 in mice causes significantly increased bone mass independent of Lrp5. In the present study, it was demonstrated that the bone-anabolic effect of Wnt1 is also independent of Fzd9. To further investigate the mechanism of Wnt1 in bone metabolism, ST2 cells, calvarial osteoblasts, bone marrow-derived osteoblasts and MC3T3 cells were stimulated with reWnt1/Sfrp1. Although these cells responded differently to the stimulation, Omd and Postn were identified as potential downstream targets that mediate the function of Wnt1 in bone metabolism. Moreover, Fzd4 was identified as a potential receptor for Wnt1. Our future studies will further investigate the mechanism of Wnt1 based on these findings.

## 6. Zusammenfassung

Der Ligand WNT1 hat sich als ein erheblicher Faktor für die Regulation der skelettale Integrität und des Knochenstoffwechsels beim Menschen erwiesen. In der Tat gibt es viele Patienten, die an Skeletterkrankungen leiden, die durch Mutationen von WNT1 verursacht werden, wie die frühmanifeste Osteoporose (EOOP) und osteogenesis imperfecta (OI). Obwohl die tatsächlichen Stoffwechselbedingungen von Mensch und Maus sehr unterschiedlich sind, ist die Untersuchung des Stoffwechsels mithilfe von Mausmodellen der erste Schritt, um die Mechanismen dieser Krankheiten und Stoffwechselaktivitäten aufzudecken. Die Aktivierung von Wnt1 bei Mäusen verursacht einen signifikanten Anstieg der Knochenmasse unabhängig von Lrp5. Darüber hinaus zeigte diese Studie, dass die knochenanabolische Wirkung von Wnt1 auch unabhängig von Fzd9 ist. Um den Mechanismus von Wnt1 im Knochenstoffwechsel weiter zu untersuchen, wurden ST2-Zellen, Schädeldach-Osteoblasten, Knochenmark-Osteoblasten und MC3T3-Zellen mit reWnt1/Sfrp1 stimuliert. Obwohl diese Zellen unterschiedlich auf die Stimulation reagierten, zeigte sich, dass Omd und Postn potenziell die nachgeschalteten Ziele sind, die die Funktion von Wnt1 im Knochenstoffwechsel vermitteln. Darüber hinaus konnte Fzd4 als potentieller Rezeptor für Wnt1 identifiziert werden. Unsere zukünftigen Studien werden den Mechanismus von Wnt1 basierend auf diesen Erkenntnissen tiefergehend untersuchen.

## 7. Abbreviations

Alpl/ALPL	Alkaline phosphatase
Ahr	Aryl hydrocarbon receptor
APC	Adenomatous polyposis coli
Apcdd1	Adenomatosis polyposis coli down-regulated 1 protein
BDB1	Brachydactyly type B
Bglap	Bone gamma-carboxyglutamic acid-containing protein
BMPs	Bone morphogenetic proteins
BMUs	Basic multicellular units
BSP/lbsp	Bone sialoprotein
BV/TV	Bone volume/tissue volume
CamKII	Calcium/calmodulin-dependent kinase II
Ccnd1	Cyclin D1
CK1	Casein kinase 1
Ct. Por	Cortical porosity
Ct. Th	Cortical thickness
Cyr61	Cysteine-rich angiogenic inducer 61
DAAM1	Dishevelled-associated activator of morphogenesis 1
DAG	Diacylglycerol
DKK1	Dickkopf-related protein 1
Dox	Doxycycline
DSH	Dishevelled
Enpp2	Ectonucleotide pyrophosphatase/phosphodiesterase family member 2
EOOP	Early-onset osteoporosis
FCS	Fetal calf serum
FGF23	Fibroblast growth factor 23
FRAT1	Frequently rearranged in advanced T-cell lymphoma 1
FZD	Frizzled
GSK3	Glycogen synthase kinase 3
IP3	Inositol triphosphate
JNK	c-Jun N-terminal kinases
LRP	Low density lipoprotein receptor-related protein
MAPKs	Mitogen-activated protein kinases
M-CSF	Macrophage colony-stimulating factor
MMP-9	Matrix metalloproteinase-9
NFAT	Nuclear factor of activated T-cells
Nkd2	Naked cuticle 2
OCN	Osteocalcin
OI	Osteogenesis imperfecta
Omd	Osteomodulin
OPG	Osteoprotegerin
OPPG	Osteoporosis-pseudoglioma syndrome
PCR	Polymerase chain reaction

PKC	Protein kinase C
Postn	Periostin
qRT-PCR	Quantitative real-time PCR
RANKL	Receptor activator of nuclear factor kappa-B ligand
ROCK	RHO-associated kinase
ROR2	Receptor tyrosine kinase-like orphan receptor 2
RRS	Robinow syndrome
Runx2	Runt-related transcription factor 2
RYK	Receptor-like tyrosine kinase
Sfrp1	Secreted frizzled related protein-1
SOST	Sclerostin
Sp7	Transcription factor Sp7
Tb. N	Trabecular number
Tb. Sp	Trabecular separation
Tb. Th	Trabecular thickness
Tb. TMD	Trabecular Tissue mineral density
TCF/LEF	T cell factor/lymphoid enhancer factor
Tnfrsf11b	Tumor necrosis factor receptor superfamily member 11b
Tnfsf11	Tumor necrosis factor ligand superfamily member 11
V-ATPase	Vacuolar proton ATPase
VBD	Van Buchem disease
WNT-Ca <sup>2+</sup> pathway	WNT-calcium pathway
WNT-PCP pathway	WNT-planar cell polarity pathway
αMEM	Minimum Essential Medium Eagle - Alpha Modification

## 8. References

1. Bilezikian JP, Martin TJ, Clemens TL, Rosen C. *Principles of Bone Biology*. Elsevier Science; 2019.
2. Clarke B. Normal bone anatomy and physiology. *Clinical journal of the American Society of Nephrology : CJASN*. Nov 2008;3 Suppl 3:S131-139.
3. Lane JM, Russell L, Khan SN. Osteoporosis. *Clinical orthopaedics and related research*. Mar 2000(372):139-150.
4. Gong Y, Slee RB, Fukai N, et al. LDL receptor-related protein 5 (LRP5) affects bone accrual and eye development. *Cell*. Nov 16 2001;107(4):513-523.
5. Forlino A, Marini JC. Osteogenesis imperfecta. *Lancet*. Apr 16 2016;387(10028):1657-1671.
6. Poole KE, van Bezooijen RL, Loveridge N, et al. Sclerostin is a delayed secreted product of osteocytes that inhibits bone formation. *FASEB journal : official publication of the Federation of American Societies for Experimental Biology*. Nov 2005;19(13):1842-1844.
7. Saito-Diaz K, Chen TW, Wang X, et al. The way Wnt works: components and mechanism. *Growth factors*. Feb 2013;31(1):1-31.
8. Laine CM, Joeng KS, Campeau PM, et al. WNT1 mutations in early-onset osteoporosis and osteogenesis imperfecta. *The New England journal of medicine*. May 9 2013;368(19):1809-1816.
9. Berendsen AD, Olsen BR. Bone development. *Bone*. Nov 2015;80:14-18.
10. Buck DW, 2nd, Dumanian GA. Bone biology and physiology: Part I. The fundamentals. *Plastic and reconstructive surgery*. Jun 2012;129(6):1314-1320.
11. Kronenberg HM. Developmental regulation of the growth plate. *Nature*. May 15 2003;423(6937):332-336.
12. Florencio-Silva R, Sasso GR, Sasso-Cerri E, Simoes MJ, Cerri PS. Biology of Bone Tissue: Structure, Function, and Factors That Influence Bone Cells. *BioMed research international*. 2015;2015:421746.
13. Guntur AR, Rosen CJ. Bone as an endocrine organ. *Endocrine practice : official journal of the American College of Endocrinology and the American Association of Clinical Endocrinologists*. Sep-Oct 2012;18(5):758-762.
14. Liu S, Guo R, Simpson LG, Xiao ZS, Burnham CE, Quarles LD. Regulation of fibroblastic growth factor 23 expression but not degradation by PHEX. *The Journal of biological chemistry*. Sep 26 2003;278(39):37419-37426.
15. Shimada T, Kakitani M, Yamazaki Y, et al. Targeted ablation of Fgf23 demonstrates an essential physiological role of FGF23 in phosphate and vitamin D metabolism. *The Journal of clinical investigation*. Feb 2004;113(4):561-568.
16. Confavreux CB. Bone: from a reservoir of minerals to a regulator of energy metabolism. *Kidney international*. Apr 2011;79(121):S14-19.
17. Oury F, Sumara G, Sumara O, et al. Endocrine regulation of male fertility by the skeleton. *Cell*. Mar 4 2011;144(5):796-809.
18. Ferron M, Hinoi E, Karsenty G, Ducy P. Osteocalcin differentially regulates beta cell and adipocyte gene expression and affects the development of metabolic diseases in wild-type mice. *Proceedings of the National Academy of Sciences of*

- the United States of America*. Apr 1 2008;105(13):5266-5270.
19. Walsh MC, Kim N, Kadono Y, et al. Osteoimmunology: interplay between the immune system and bone metabolism. *Annual review of immunology*. 2006;24:33-63.
  20. Capulli M, Paone R, Rucci N. Osteoblast and osteocyte: games without frontiers. *Archives of biochemistry and biophysics*. Nov 1 2014;561:3-12.
  21. Boivin G, Meunier PJ. The degree of mineralization of bone tissue measured by computerized quantitative contact microradiography. *Calcified tissue international*. Jun 2002;70(6):503-511.
  22. Jilka RL, Weinstein RS, Bellido T, Parfitt AM, Manolagas SC. Osteoblast programmed cell death (apoptosis): modulation by growth factors and cytokines. *Journal of bone and mineral research : the official journal of the American Society for Bone and Mineral Research*. May 1998;13(5):793-802.
  23. Matic I, Matthews BG, Wang X, et al. Quiescent Bone Lining Cells Are a Major Source of Osteoblasts During Adulthood. *Stem cells*. Dec 2016;34(12):2930-2942.
  24. Mullender MG, van der Meer DD, Huiskes R, Lips P. Osteocyte density changes in aging and osteoporosis. *Bone*. Feb 1996;18(2):109-113.
  25. Nakashima T, Hayashi M, Fukunaga T, et al. Evidence for osteocyte regulation of bone homeostasis through RANKL expression. *Nature medicine*. Sep 11 2011;17(10):1231-1234.
  26. Yavropoulou MP, Yovos JG. Osteoclastogenesis--current knowledge and future perspectives. *Journal of musculoskeletal & neuronal interactions*. Jul-Sep 2008;8(3):204-216.
  27. Boyce BF, Xing L. Functions of RANKL/RANK/OPG in bone modeling and remodeling. *Archives of biochemistry and biophysics*. May 15 2008;473(2):139-146.
  28. Luxenburg C, Geblinger D, Klein E, et al. The architecture of the adhesive apparatus of cultured osteoclasts: from podosome formation to sealing zone assembly. *PloS one*. Jan 31 2007;2(1):e179.
  29. Blair HC, Athanasou NA. Recent advances in osteoclast biology and pathological bone resorption. *Histology and histopathology*. Jan 2004;19(1):189-199.
  30. Datta HK, Ng WF, Walker JA, Tuck SP, Varanasi SS. The cell biology of bone metabolism. *Journal of clinical pathology*. May 2008;61(5):577-587.
  31. Downey PA, Siegel MI. Bone biology and the clinical implications for osteoporosis. *Physical therapy*. Jan 2006;86(1):77-91.
  32. Xiong J, Onal M, Jilka RL, Weinstein RS, Manolagas SC, O'Brien CA. Matrix-embedded cells control osteoclast formation. *Nature medicine*. Sep 11 2011;17(10):1235-1241.
  33. Sharma RP, Chopra VL. Effect of the Wingless (wg1) mutation on wing and haltere development in *Drosophila melanogaster*. *Developmental biology*. Feb 1976;48(2):461-465.
  34. Nusse R, Varmus HE. Many tumors induced by the mouse mammary tumor virus contain a provirus integrated in the same region of the host genome. *Cell*. Nov 1982;31(1):99-109.
  35. Rijsewijk F, Schuermann M, Wagenaar E, Parren P, Weigel D, Nusse R. The

- Drosophila homolog of the mouse mammary oncogene int-1 is identical to the segment polarity gene wingless. *Cell*. Aug 14 1987;50(4):649-657.
36. Nusse R, Brown A, Papkoff J, et al. A new nomenclature for int-1 and related genes: the Wnt gene family. *Cell*. Jan 25 1991;64(2):231.
  37. Baron R, Kneissel M. WNT signaling in bone homeostasis and disease: from human mutations to treatments. *Nature medicine*. Feb 2013;19(2):179-192.
  38. Lerner UH, Ohlsson C. The WNT system: background and its role in bone. *Journal of internal medicine*. Jun 2015;277(6):630-649.
  39. Cadigan KM, Peifer M. Wnt signaling from development to disease: insights from model systems. *Cold Spring Harbor perspectives in biology*. Aug 2009;1(2):a002881.
  40. Ng LF, Kaur P, Bunnag N, et al. WNT Signaling in Disease. *Cells*. Aug 3 2019;8(8).
  41. Gao B. Wnt regulation of planar cell polarity (PCP). *Current topics in developmental biology*. 2012;101:263-295.
  42. Ishitani T, Kishida S, Hyodo-Miura J, et al. The TAK1-NLK mitogen-activated protein kinase cascade functions in the Wnt-5a/Ca(2+) pathway to antagonize Wnt/beta-catenin signaling. *Molecular and cellular biology*. Jan 2003;23(1):131-139.
  43. Holmen SL, Giambernardi TA, Zylstra CR, et al. Decreased BMD and limb deformities in mice carrying mutations in both Lrp5 and Lrp6. *Journal of bone and mineral research : the official journal of the American Society for Bone and Mineral Research*. Dec 2004;19(12):2033-2040.
  44. Leupin O, Piters E, Halleux C, et al. Bone overgrowth-associated mutations in the LRP4 gene impair sclerostin facilitator function. *The Journal of biological chemistry*. Jun 3 2011;286(22):19489-19500.
  45. Johnson EB, Hammer RE, Herz J. Abnormal development of the apical ectodermal ridge and polysyndactyly in Megf7-deficient mice. *Human molecular genetics*. Nov 15 2005;14(22):3523-3538.
  46. Wang B, Sinha T, Jiao K, Serra R, Wang J. Disruption of PCP signaling causes limb morphogenesis and skeletal defects and may underlie Robinow syndrome and brachydactyly type B. *Human molecular genetics*. Jan 15 2011;20(2):271-285.
  47. Kennell JA, MacDougald OA. Wnt signaling inhibits adipogenesis through beta-catenin-dependent and -independent mechanisms. *The Journal of biological chemistry*. Jun 24 2005;280(25):24004-24010.
  48. Day TF, Guo X, Garrett-Beal L, Yang Y. Wnt/beta-catenin signaling in mesenchymal progenitors controls osteoblast and chondrocyte differentiation during vertebrate skeletogenesis. *Developmental cell*. May 2005;8(5):739-750.
  49. Hill TP, Spater D, Taketo MM, Birchmeier W, Hartmann C. Canonical Wnt/beta-catenin signaling prevents osteoblasts from differentiating into chondrocytes. *Developmental cell*. May 2005;8(5):727-738.
  50. Maeda K, Kobayashi Y, Udagawa N, et al. Wnt5a-Ror2 signaling between osteoblast-lineage cells and osteoclast precursors enhances osteoclastogenesis. *Nature medicine*. Feb 19 2012;18(3):405-412.
  51. Pederson L, Ruan M, Westendorf JJ, Khosla S, Oursler MJ. Regulation of bone formation by osteoclasts involves Wnt/BMP signaling and the chemokine

- sphingosine-1-phosphate. *Proceedings of the National Academy of Sciences of the United States of America*. Dec 30 2008;105(52):20764-20769.
52. Stevens JR, Miranda-Carboni GA, Singer MA, Brugger SM, Lyons KM, Lane TF. Wnt10b deficiency results in age-dependent loss of bone mass and progressive reduction of mesenchymal progenitor cells. *Journal of bone and mineral research : the official journal of the American Society for Bone and Mineral Research*. Oct 2010;25(10):2138-2147.
  53. Bennett CN, Ouyang H, Ma YL, et al. Wnt10b increases postnatal bone formation by enhancing osteoblast differentiation. *Journal of bone and mineral research : the official journal of the American Society for Bone and Mineral Research*. Dec 2007;22(12):1924-1932.
  54. Isojima T, Sims NA. Cortical bone development, maintenance and porosity: genetic alterations in humans and mice influencing chondrocytes, osteoclasts, osteoblasts and osteocytes. *Cellular and molecular life sciences : CMLS*. Jul 1 2021.
  55. Hendrickx G, Boudin E, Verbeek M, Fransen E, Mortier G, Van Hul W. WNT16 Requires Galpha Subunits as Intracellular Partners for Both Its Canonical and Non-Canonical WNT Signalling Activity in Osteoblasts. *Calcified tissue international*. Mar 2020;106(3):294-302.
  56. Luther J, Yorgan TA, Rolvien T, et al. Wnt1 is an Lrp5-independent bone-anabolic Wnt ligand. *Science translational medicine*. Nov 7 2018;10(466).
  57. Clevers H, Nusse R. Wnt/beta-catenin signaling and disease. *Cell*. Jun 8 2012;149(6):1192-1205.
  58. Fahiminiya S, Majewski J, Mort J, Moffatt P, Glorieux FH, Rauch F. Mutations in WNT1 are a cause of osteogenesis imperfecta. *Journal of medical genetics*. May 2013;50(5):345-348.
  59. Keupp K, Beleggia F, Kayserili H, et al. Mutations in WNT1 cause different forms of bone fragility. *American journal of human genetics*. Apr 4 2013;92(4):565-574.
  60. Albers J, Schulze J, Beil FT, et al. Control of bone formation by the serpentine receptor Frizzled-9. *The Journal of cell biology*. Mar 21 2011;192(6):1057-1072.
  61. Takahashi M, Fujita M, Furukawa Y, et al. Isolation of a novel human gene, APCDD1, as a direct target of the beta-Catenin/T-cell factor 4 complex with probable involvement in colorectal carcinogenesis. *Cancer research*. Oct 15 2002;62(20):5651-5656.
  62. Schneider AJ, Branam AM, Peterson RE. Intersection of AHR and Wnt signaling in development, health, and disease. *International journal of molecular sciences*. Oct 3 2014;15(10):17852-17885.
  63. Richards JS, Fan HY, Liu Z, et al. Either Kras activation or Pten loss similarly enhance the dominant-stable CTNNB1-induced genetic program to promote granulosa cell tumor development in the ovary and testis. *Oncogene*. Mar 22 2012;31(12):1504-1520.
  64. Li ZQ, Ding W, Sun SJ, et al. Cyr61/CCN1 is regulated by Wnt/beta-catenin signaling and plays an important role in the progression of hepatocellular carcinoma. *PloS one*. 2012;7(4):e35754.
  65. Loots GG, Kneissel M, Keller H, et al. Genomic deletion of a long-range bone enhancer misregulates sclerostin in Van Buchem disease. *Genome research*. Jul

- 2005;15(7):928-935.
66. Balemans W, Patel N, Ebeling M, et al. Identification of a 52 kb deletion downstream of the SOST gene in patients with van Buchem disease. *Journal of medical genetics*. Feb 2002;39(2):91-97.
  67. Thomas KR, Capecchi MR. Targeted disruption of the murine int-1 proto-oncogene resulting in severe abnormalities in midbrain and cerebellar development. *Nature*. Aug 30 1990;346(6287):847-850.
  68. McMahon AP, Bradley A. The Wnt-1 (int-1) proto-oncogene is required for development of a large region of the mouse brain. *Cell*. Sep 21 1990;62(6):1073-1085.
  69. Thomas KR, Musci TS, Neumann PE, Capecchi MR. Swaying is a mutant allele of the proto-oncogene Wnt-1. *Cell*. Nov 29 1991;67(5):969-976.
  70. Joeng KS, Lee YC, Jiang MM, et al. The swaying mouse as a model of osteogenesis imperfecta caused by WNT1 mutations. *Human molecular genetics*. Aug 1 2014;23(15):4035-4042.
  71. Lu Y, Ren X, Wang Y, et al. Novel WNT1 mutations in children with osteogenesis imperfecta: Clinical and functional characterization. *Bone*. Sep 2018;114:144-149.
  72. Yorgan TA, Rolvien T, Sturznickel J, et al. Mice Carrying a Ubiquitous R235W Mutation of Wnt1 Display a Bone-Specific Phenotype. *Journal of bone and mineral research : the official journal of the American Society for Bone and Mineral Research*. Sep 2020;35(9):1726-1737.
  73. Joeng KS, Schumacher CA, Zylstra-Diegel CR, Long F, Williams BO. Lrp5 and Lrp6 redundantly control skeletal development in the mouse embryo. *Developmental biology*. Nov 15 2011;359(2):222-229.
  74. Katoh M, Katoh M. WNT signaling pathway and stem cell signaling network. *Clinical cancer research : an official journal of the American Association for Cancer Research*. Jul 15 2007;13(14):4042-4045.
  75. Shimomura Y, Agalliu D, Vonica A, et al. APCDD1 is a novel Wnt inhibitor mutated in hereditary hypotrichosis simplex. *Nature*. Apr 15 2010;464(7291):1043-1047.
  76. Sah JP, Hao NTT, Han X, et al. Ectonucleotide pyrophosphatase 2 (ENPP2) plays a crucial role in myogenic differentiation through the regulation by WNT/beta-Catenin signaling. *The international journal of biochemistry & cell biology*. Jan 2020;118:105661.
  77. Si W, Kang Q, Luu HH, et al. CCN1/Cyr61 is regulated by the canonical Wnt signal and plays an important role in Wnt3A-induced osteoblast differentiation of mesenchymal stem cells. *Molecular and cellular biology*. Apr 2006;26(8):2955-2964.
  78. Bonnet N, Conway SJ, Ferrari SL. Regulation of beta catenin signaling and parathyroid hormone anabolic effects in bone by the extracellular matrix protein periostin. *Proceedings of the National Academy of Sciences of the United States of America*. Sep 11 2012;109(37):15048-15053.
  79. Bonnet N, Gineyts E, Ammann P, Conway SJ, Garnero P, Ferrari S. Periostin deficiency increases bone damage and impairs injury response to fatigue loading in adult mice. *PLoS one*. 2013;8(10):e78347.
  80. Bonnet N, Garnero P, Ferrari S. Periostin action in bone. *Molecular and cellular*

- endocrinology*. Sep 5 2016;432:75-82.
81. Gerbaix M, Vico L, Ferrari SL, Bonnet N. Periostin expression contributes to cortical bone loss during unloading. *Bone*. Feb 2015;71:94-100.
  82. Tashima T, Nagatoishi S, Sagara H, Ohnuma S, Tsumoto K. Osteomodulin regulates diameter and alters shape of collagen fibrils. *Biochemical and biophysical research communications*. Jul 31 2015;463(3):292-296.
  83. Tashima T, Nagatoishi S, Caaveiro JMM, et al. Molecular basis for governing the morphology of type-I collagen fibrils by Osteomodulin. *Communications biology*. 2018;1:33.
  84. Rehn AP, Cerny R, Sugars RV, Kaukua N, Wendel M. Osteoadherin is upregulated by mature osteoblasts and enhances their in vitro differentiation and mineralization. *Calcified tissue international*. Jun 2008;82(6):454-464.
  85. Ramstad VE, Franzen A, Heinegard D, Wendel M, Reinholt FP. Ultrastructural distribution of osteoadherin in rat bone shows a pattern similar to that of bone sialoprotein. *Calcified tissue international*. Jan 2003;72(1):57-64.
  86. Hatsumi T, Yamamuro Y. Downregulation of estrogen receptor gene expression by exogenous 17beta-estradiol in the mammary glands of lactating mice. *Experimental biology and medicine*. Mar 2006;231(3):311-316.
  87. Kushwaha P, Kim S, Foxa GE, et al. Frizzled-4 is required for normal bone acquisition despite compensation by Frizzled-8. *Journal of cellular physiology*. Oct 2020;235(10):6673-6683.
  88. Albers J, Keller J, Baranowsky A, et al. Canonical Wnt signaling inhibits osteoclastogenesis independent of osteoprotegerin. *The Journal of cell biology*. Feb 18 2013;200(4):537-549.

## **9. Acknowledgements**

Hereby I express my sincere thanks to my supervisors Prof. Dr. Michael Amling and Prof. Dr. Thorsten Schinke, who gave me a valuable opportunity to join IOBM and always support me on the projects. I also would like to thank my co-supervisor PD Dr. Timur Yorgan, who gives me a lot of help in both science and daily life. It's a great pleasure to work with you.

I am so glad that I have lots of outstanding and nice colleagues in our group. I really enjoy working with you all. I want to thank my colleagues, Dr. Anke Baranowsky, Dr. Julia Luther, Dr. Laura Brylka, Armelle Carreau, Philip Wiedemann, Mona Neven, Lana Rosenthal, and my colleagues in the lab at Lottestraße. Although some colleagues have finished working in our group and left, I am very happy that we had a wonderful time working together. Here I also express my thanks to Dr. Nannan Liao, Dr. Gretl Hendrickx, Dr. Julian Peterson, Dr. Maximilian Decker and Dr. Cita Nottmeier.

I am grateful to all my friends who help and support me. And I want to thank my families, who always support me and encourage me in every aspect of life.

## 10. Publications

1. Yorgan TA, Rolvien T, Stürznickel J, Vollersen N, Lange F, **Zhao W**, Baranowsky A, Rosenthal L, Hermans-Borgmeyer I, Sharaf A, Karsak M, David JP, Oheim R, Amling M, Schinke T. Mice Carrying a Ubiquitous R235W Mutation of Wnt1 Display a Bone-Specific Phenotype. *J Bone Miner Res.* 2020 Sep;35(9):1726-1737. doi: 10.1002/jbmr.4043.
2. Vollersen N \*, **Zhao W** \*, Rolvien T, Lange F, Schmidt FN, Sonntag S, Shmerling D, von Kroge S, Stockhausen KE, Sharaf A, Schweizer M, Karsak M, Busse B, Bockamp E, Semler O, Amling M, Oheim R, Schinke T, Yorgan TA. The WNT1<sup>G177C</sup> mutation specifically affects skeletal integrity in a mouse model of osteogenesis imperfecta type XV. *Bone Res.* Accepted in July, 2021.  
(\* co-first authors)

## 11. Lebenslauf

Name: Wenbo Zhao

Date of birth: 25.05.1993

Place of birth: Kunming, P.R. China

### Education (since middle school)

- 09.2005~06.2008 Yunnan University Secondary School, Kunming, P.R. China  
09.2008~06.2011 Kunming No.1 High School, Kunming, P.R. China  
09.2011~06.2016 Shanghai Jiao Tong University School of Medicine, Shanghai, P.R. China  
Bachelor Degree of Medicine  
08.2016~06.2019 Shanghai Jiao Tong University School of Medicine, Shanghai, P.R. China  
Master Degree of Medicine  
Major: Surgery  
Since 10.2019 Department of Osteology and Biomechanics, University Medical Center Hamburg-Eppendorf, Hamburg, Germany

### Training

- 05.2015~05.2016 Renji Hospital, Shanghai Jiao Tong University School of Medicine, Shanghai, P.R. China  
Clinical internship  
08.2016~08.2019 Renji Hospital, Shanghai Jiao Tong University School of Medicine, Shanghai, P.R. China  
Resident training

### Publications

1. Jin X \*, **Zhao W** \*, Dong Y, Huang Y. Simultaneous dislocation of the radial head and distal radio-ulnar joint without fracture in an adult patient: a case report and review of literature. *BMC Surg.* 2020 Apr 15;20(1):71. doi: 10.1186/s12893-020-00717-8
2. Yorgan TA, Rolvien T, Stürznickel J, Vollersen N, Lange F, **Zhao W**, Baranowsky A, Rosenthal L, Hermans-Borgmeyer I, Sharaf A, Karsak M, David JP, Oheim R, Amling M, Schinke T. Mice Carrying a Ubiquitous R235W Mutation of Wnt1 Display a Bone-Specific Phenotype. *J Bone Miner Res.* 2020 Sep;35(9):1726-1737. doi: 10.1002/jbmr.4043.
3. Vollersen N \*, **Zhao W** \*, Rolvien T, Lange F, Schmidt FN, Sonntag S, Shmerling D, von Kroge S, Stockhausen KE, Sharaf A, Schweizer M, Karsak M, Busse B, Bockamp E, Semler O, Amling M, Oheim R, Schinke T, Yorgan TA. The WNT1<sup>G177C</sup> mutation specifically affects skeletal integrity in a mouse model of osteogenesis imperfecta type XV. *Bone Res.* Accepted in July, 2021.  
(\* co-first authors)

## **12. Eidesstattliche Versicherung**

Ich versichere ausdrücklich, dass ich die Arbeit selbständig und ohne fremde Hilfe verfasst, andere als die von mir angegebenen Quellen und Hilfsmittel nicht benutzt und die aus den benutzten Werken wörtlich oder inhaltlich entnommenen Stellen einzeln nach Ausgabe (Auflage und Jahr des Erscheinens), Band und Seite des benutzten Werkes kenntlich gemacht habe.

Ferner versichere ich, dass ich die Dissertation bisher nicht einem Fachvertreter an einer anderen Hochschule zur Überprüfung vorgelegt oder mich anderweitig um Zulassung zur Promotion beworben habe.

Ich erkläre mich einverstanden, dass meine Dissertation vom Dekanat der Medizinischen Fakultät mit einer gängigen Software zur Erkennung von Plagiaten überprüft werden kann.

Unterschrift: .....